ELSEVIER

Journal of Fluids and Structures 25 (2009) 205–227

JOURNAL OF FLUIDS AND STRUCTURES

www.elsevier.com/locate/jfs

On forced flow through a baffled wall aperture, with application to compression wave generation in a tunnel

M.S. Howe[a,*], M. Iida[b], T. Miyachi[b]

[a]*College of Engineering, Boston University, 110 Cummington Street, Boston, MA 02215, USA*
[b]*Railway Technical Research Institute, 2-8-38 Hikari-cho, Kokubunji-shi, Tokyo 185-8540, Japan*

Received 6 December 2007; accepted 1 June 2008

Abstract

An analysis is made of the sound produced by vorticity generated as high pressure fluid is forced through an aperture in the wall of a duct in the presence of an exterior baffle plate. The aperture typically behaves as a 'pressure release' opening when the flow is ideal and irrotational, corresponding to the traditional interpretation of the action of a finger hole of a woodwind instrument, although theoretical predictions that neglect vorticity are irrelevant in practice except at very high frequencies. The theory of vortex sound is applied to derive an approximate nonlinear equation for the volume flux through the baffled aperture that generalises Cummings's empirical equation for a jet exhausting through a fully open orifice in a large wall. The equation takes account of the impingement of the jet on the baffle and of the nonlinear 'inertial blocking' of the aperture flow. Application is made to the problem of compression wave generation by a high-speed train entering a tunnel fitted with an entrance hood whose windows are partially 'closed' by the presence of a side-wall of a railway cutting or embankment. Theoretical predictions are found to be in good agreement with measurements made at model scale at train speeds $\sim 300-400\,\mathrm{km/h}$.

1. Introduction

Perforated splitter plates and cavity covers are frequently used in vibration control and to suppress acoustic noise [see e.g. Cummings (1984, 1986), Howe (1979a, b, 1998a), Hughes and Dowling (1990), Salikuddin and Plumlee (1980), Salikuddin (1990) and Vér (1990)]. But vorticity generated during unsteady high Reynolds number flow through an aperture can also be a powerful source of sound (Howe, 1998a; Howe et al., 2003a; Howe and McGowan, 2007). The hydrodynamics of such flows govern the influence of the partial opening of 'finger holes' on the fine tuning of a woodwind instrument (Benade, 1976; Leppington, 1982). A very important application at a much larger scale is the use of relatively large apertures or 'windows' in the side-wall of a railway tunnel, usually near the tunnel portal, to alter the waveform of the low frequency compression wave generated by a high-speed train entering the tunnel (Ozawa and Maeda, 1988; Ozawa et al., 1991; Maeda, 2002). All of these acoustic effects depend for their action on the presence of vorticity in the aperture outflow.

The amplitude of the compression wave generated as a high-speed train enters a tunnel is frequently as large as 2% or 3% of atmospheric pressure. Uncontrolled nonlinear steepening of the wave as it propagates ahead of the train in the

*Corresponding author.
E-mail address: mshowe@bu.edu (M.S. Howe).

0889-9746/$ - see front matter © 2008 Elsevier Ltd. All rights reserved.
doi:10.1016/j.jfluidstructs.2008.06.002

tunnel can increase the discomfort to passengers and personnel within the tunnel, and produces the 'micro-pressure wave' often observed to be radiated from the distant tunnel exit in the form of a subjectively annoying 'crack' or 'bang'. The principal practical method of suppressing this wave involves modification of the portal where the train enters the tunnel so that the initial pressure rise across the wavefront is sufficiently 'stretched-out' that nonlinear steepening becomes ineffective (Ozawa et al., 1978; Ozawa and Maeda, 1988, 1998; Maeda et al., 1993; Maeda, 2002; Howe et al., 2003b, 2006; Howe, 2007).

The modified portal usually is formed by the addition of a 'hood', consisting of a thin-walled tunnel extension placed ahead of the tunnel entrance. The 'rise time' of the compression wave formed as a train enters the hood can be increased by permitting high pressure air in front of the train to exhaust through one or more windows in the hood walls. The air leaves the window in the form of a high-speed jet (with velocity often exceeding half that of the train). Experimental design studies and analyses have usually assumed that the jet flows freely into the ambient atmosphere (Howe et al., 2006). In practice, however, the hood is often sited within a railway 'cutting' with windows facing the cutting wall; an air jet forced out of the window must then impinge on the wall and produce a change in the window's acoustic properties that are analogous to those of a partially closed finger hole.

In this paper we consider both theoretically and experimentally the aeroacoustics of a wall-baffled aperture of this kind, for an aperture in a uniform duct in the presence of a parallel, exterior baffle plate. The problem of sound generation by impingement of the jet on the baffle is formulated in Section 2 as a problem in the theory of vortex sound (Howe, 1998a; Howe et al., 2000). The influence of the baffle on the propagation of low frequency sound in the duct is discussed in Section 3. Application is then made to the problem of compression wave generation by a high-speed train (Section 4) and predictions of the influence of a baffled window are compared with model scale test results (at train speeds $\sim 300-400\,\mathrm{km/h}$) in Section 5.

2. Aeroacoustics of the aperture

2.1. Governing equations

Consider a cylindrical hard-walled duct of rectangular cross-section of area $\mathscr{A}$ having walls of uniform thickness ℓ_w. There is a circular aperture of radius R_w and area $\mathscr{A}_w = \pi R_w^2 \ll \mathscr{A}$ in one of the walls. Take coordinate axes $\mathbf{x} = (x_1, x_2, x_3)$ with the origin at the centre of the inner face of the aperture, the x_1-axis parallel to the duct (Fig. 1), and with the x_3-axis directed 'inwards' from the aperture. The exterior face of the aperture is 'covered' by a parallel rigid, concentric circular wall or baffle plate of radius D at a perpendicular standoff distance d from the outer face, where D is assumed to be smaller than the width of the adjacent duct wall.

The fluid within the duct is at rest in the mean and is homogeneous with mean density ρ_0 and sound speed c_0. The Mach number of any unsteady motions is sufficiently small for the flow to be regarded as isentropic and for the propagation and generation of sound to be governed by Lighthill's (1952) equation in the form (Howe, 1998a, 2003)

$$\left(\frac{1}{c_0^2}\frac{\partial^2}{\partial t^2} - \nabla^2\right) B = \mathrm{div}(\boldsymbol{\omega} \wedge \mathbf{v}), \tag{2.1}$$

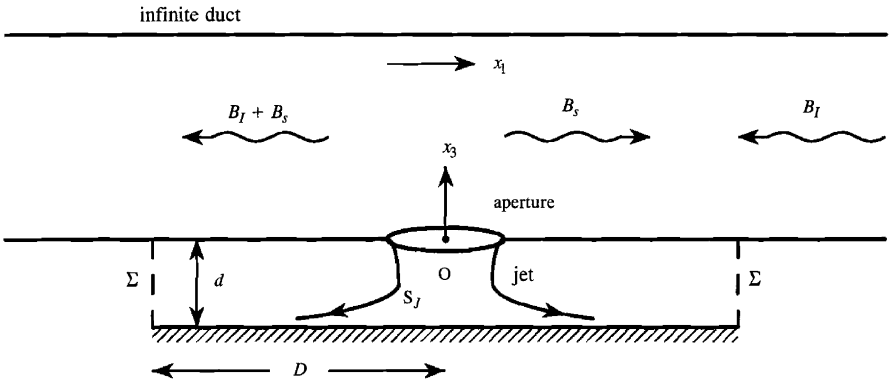

Fig. 1. Scattering of low frequency sound in an infinite duct with circular wall aperture and exterior circular panel.

where t denotes time, $\mathbf{v}$ is the fluid velocity, $\boldsymbol{\omega} = \operatorname{curl}\mathbf{v}$ is the vorticity, and the acoustic variable is the total enthalpy B. In the present case of isentropic motion we can put $B = \int \mathrm{d}p/\rho + \frac{1}{2}v^2$, because fluctuations in the density ρ are determined by changes in the pressure p. In the absence of vorticity $B = -\partial\varphi/\partial t + \text{constant}$, where φ is the velocity potential of the motion. In the absence of flow B may be assumed to vanish.

A plane acoustic wave $B_I(t + x_1/c_0)$ satisfying the homogeneous form of (2.1) is incident on the aperture from $x_1 = +\infty$. The disturbance B_s in the duct scattered from the aperture is an out-going solution of (2.1) including source terms involving vorticity produced by the 'jetting' of fluid forced through the aperture by the incident wave. To determine B_s Green's function $G(\mathbf{x}, \mathbf{y}, t-\tau)$ is introduced that satisfies

$$\left(\frac{1}{c_0^2}\frac{\partial^2}{\partial t^2} - \nabla^2\right) G = \delta(\mathbf{x}-\mathbf{y})\delta(t-\tau), \quad G = 0 \text{ for } t < \tau, \tag{2.2}$$

within the duct and aperture and within the region between the external wall of the duct and the baffle. G is required to have vanishing normal derivatives on the duct walls and on the baffle and to vanish at the circular cylindrical opening $\varpi \equiv \sqrt{x_1^2 + x_2^2} = D$ (Σ in Fig. 1) at the outer circumference of the circular baffle plate. The latter corresponds to the low frequency approximation in which the escape of acoustic energy from the duct through the aperture to the ambient free space is ignored.

The usual procedure involving the application of Green's theorem and the radiation condition to Eq. (2.1) with B replaced by B_s, and Eq. (2.2) permits B_s to be expressed in the form (Baker and Copson, 1969; Landau and Lifshitz, 1987; Crighton et al., 1992; Howe, 1998a)

$$\begin{aligned} B_s(\mathbf{x}, t) = & -\oint_{S+\Sigma} \left(G(\mathbf{x}, \mathbf{y}, t-\tau)\frac{\partial B_s}{\partial y_j}(\mathbf{y}, \tau) - B_s(\mathbf{y}, \tau)\frac{\partial G}{\partial y_j}(\mathbf{x}, \mathbf{y}, t-\tau)\right) \mathrm{d}S_j(\mathbf{y})\,\mathrm{d}\tau \\ & + \int G(\mathbf{x}, \mathbf{y}, t-\tau)\frac{\partial}{\partial y_j}(\boldsymbol{\omega}\wedge\mathbf{v})_j(\mathbf{y}, \tau)\,\mathrm{d}^3\mathbf{y}\,\mathrm{d}\tau, \end{aligned} \tag{2.3}$$

where the integration is over all values of the source time $-\infty < \tau < +\infty$, the surface integral is over the region S consisting of the interior wall of the duct and the solid boundaries of the region between the baffle and the exterior duct wall (with surface element $\mathrm{d}\mathbf{S}$ directed *into* the fluid), and over the circular cylindrical control surface Σ; the volume integral is over the fluid regions occupied by vorticity.

Crocco's form of the momentum equation consistent with approximation (2.1) (Howe, 1998a)

$$\frac{\partial \mathbf{v}}{\partial t} + \nabla B = -\boldsymbol{\omega}\wedge\mathbf{v} - \nu \operatorname{curl}\boldsymbol{\omega}, \tag{2.4}$$

where $B = B_I + B_s$ and ν is the kinematic viscosity can be used to simplify the integrals in (2.3). Viscosity can usually be ignored in high Reynolds number flows of aeroacoustic relevance. The contribution to (2.4) from the bulk viscosity has therefore been neglected, because its effect is small everywhere. On the other hand, the shear viscosity is responsible for possibly significant frictional boundary forces and is usually retained. In what follows, however, it will be assumed that the Reynolds number is sufficiently large that the predominant influence of viscosity is to facilitate the release of vorticity from the edges of the aperture leading to the formation of the jet in Fig. 1. This can be handled formally by imposing a Kutta condition at the aperture edges (Crighton, 1985), and henceforth the explicit contribution from surface friction will be ignored.

Then, application of the divergence theorem to the vortex integral in (2.3) and use of (2.4) and the condition $B = B_I + B_s = 0$ on Σ permit B_s to be expressed in the form

$$\begin{aligned} B_s(\mathbf{x}, t) = & -\oint_{\Sigma} B_I(\tau)\frac{\partial G}{\partial y_j}(\mathbf{x}, \mathbf{y}, t-\tau)\,\mathrm{d}S_j(\mathbf{y})\,\mathrm{d}\tau + \oint_{S} G(\mathbf{x}, \mathbf{y}, t-\tau)\left(\frac{\partial v_j}{\partial \tau} + \frac{\partial B_I}{\partial y_j}\right)(\mathbf{y}, \tau)\,\mathrm{d}S_j(\mathbf{y})\,\mathrm{d}\tau \\ & - \int (\boldsymbol{\omega}\wedge\mathbf{v})_j(\mathbf{y}, \tau)\frac{\partial G}{\partial y_j}(\mathbf{x}, \mathbf{y}, t-\tau)\,\mathrm{d}^3\mathbf{y}\,\mathrm{d}\tau \\ \equiv & -\oint_{\Sigma} B_I(\tau)\frac{\partial G}{\partial y_j}(\mathbf{x}, \mathbf{y}, t-\tau)\,\mathrm{d}S_j(\mathbf{y})\,\mathrm{d}\tau - \int (\boldsymbol{\omega}\wedge\mathbf{v})_j(\mathbf{y}, \tau)\frac{\partial G}{\partial y_j}(\mathbf{x}, \mathbf{y}, t-\tau)\,\mathrm{d}^3\mathbf{y}\,\mathrm{d}\tau, \end{aligned} \tag{2.5}$$

where the final line follows because the normal component of velocity and the normal derivative of the incident plane wave both vanish on S.

2.2. Formal solution

Only plane waves can propagate in the duct when the characteristic wavelength of the sound is large compared to its diameter $\sim\sqrt{\mathscr{A}}$. It is shown in Appendix A that in this limit the leading approximation to Green's function is

$$G(\mathbf{x},\mathbf{y},t-\tau)\approx\frac{c_0}{2\mathscr{A}}\left\{1-\frac{\varphi^*(\mathbf{y})}{\mathscr{L}}\right\}\mathrm{H}\left(t-\tau-\frac{|x_1|}{c_0}\right)\exp\left[\frac{-c_0\mathscr{A}_w}{2\mathscr{L}\mathscr{A}}\left(t-\tau-\frac{|x_1|}{c_0}\right)\right],\quad |x_1|\gg\sqrt{\mathscr{A}},\tag{2.6}$$

when the source point $\mathbf{y}$ is in the neighbourhood of the aperture and the field point $\mathbf{x}$ is *within the duct* at distances $|\mathbf{x}|\gg\sqrt{\mathscr{A}}$. In the long wavelength limit the principal contributions to the sound consist of the monopole and dipole components in a formal multipole expansion of the acoustic field. Approximation (2.6) determines these components, which correspond, respectively, to the first and second terms in the curly brackets. The function $\varphi^*(\mathbf{y})$ is a velocity potential that describes a hypothetical incompressible flow from the duct through the aperture. It satisfies Laplace's equation and is normalised to have the following asymptotic behaviours:

$$\varphi^*(\mathbf{y})\sim\begin{cases}\dfrac{\mathscr{A}_w}{2\pi r} & \text{for } |\mathbf{y}|\equiv r\gg R_w \text{ in the duct above the aperture,}\\[2ex] \dfrac{\mathscr{A}_w}{2\pi d}\ln\left(\dfrac{\varpi}{R_w}\right)+\ell & \text{for } (y_1^2+y_2^2)^{1/2}\equiv\varpi\gg R_w \text{ between the outer duct wall and the baffle,}\end{cases}\tag{2.7}$$

where the length $\ell\sim\mathscr{O}(R_w)$ is the aperture 'end correction' [discussed in Appendix A; Howe (1998a) and Rayleigh (1926)], and

$$\mathscr{L}=\frac{\mathscr{A}_w}{2\pi d}\ln\left(\frac{D}{R_w}\right)+\ell.\tag{2.8}$$

Let the incident wave correspond to an acoustic pressure $p=p_I(t+x_1/c_0)$, so that $B_I=p_I/\rho_0$, with characteristic wavelength large compared to the duct diameter and also relative to the radius D of the baffle. Then $B_I=p_I(t)/\rho_0$ in the surface integral over Σ in (2.5), which then becomes

$$\begin{aligned}p_s(\mathbf{x},t)\equiv p_s\left(t-\frac{|x_1|}{c_0}\right)&=-\frac{c_0\mathscr{A}_w}{2\mathscr{A}\mathscr{L}}\int_{-\infty}^{[t]}p_I(\tau)\exp\left[\frac{-c_0\mathscr{A}_w}{2\mathscr{A}\mathscr{L}}([t]-\tau)\right]\mathrm{d}\tau\\&+\frac{\rho_0c_0}{2\mathscr{A}\mathscr{L}}\int_{-\infty}^{[t]}\int(\boldsymbol{\omega}\wedge\mathbf{v}\cdot\nabla\varphi^*)(\mathbf{y},\tau)\exp\left[\frac{-c_0\mathscr{A}_w}{2\mathscr{A}\mathscr{L}}([t]-\tau)\right]\mathrm{d}^3\mathbf{y}\,\mathrm{d}\tau,\quad |x_1|\gg\sqrt{\mathscr{A}},\end{aligned}\tag{2.9}$$

where $p_s=B_s/\rho_0$ and $[t]=t-|x_1|/c_0$ is the retarded time.

2.3. Nonlinear differential equation for the sound

The first integral in this formula represents the pressure scattered from the aperture in ideal flow, when vorticity production in the aperture is ignored. Except at very high frequencies a pressure rise in the duct produced by an incident wave actually forces high Reynolds number flow through the aperture causing separation at the aperture edges and the formation of a jet that in a first approximation strikes the baffle plate axisymmetrically, as implied in Fig. 1. The jet shear layer is unstable and the ordered picture in this figure is not generally maintained as the flow spreads out in the region between the duct and the baffle plate, where the shear layer thickens and the flow becomes turbulent. However, the resulting small scale turbulence cannot affect the dominant characteristics of the low frequency sound in the duct, determined by the final integral of (2.9).

Fig. 2 illustrates the typical streamline pattern of the hypothetical flow defined by the function φ^* in the second integrand of (2.9). Sound is generated strongly in regions where $|\nabla\varphi^*|$ is large and rapidly varying on scales comparable to those of the jet vorticity. This occurs close to the aperture edges: at larger distances the streamlines become uniformly spaced and parallel, so that $\nabla\varphi^*\sim$ constant and the overall contribution from random vorticity between the duct and baffle tends to be very small.

At high Reynolds number it may be assumed that the shed vorticity is initially confined to 'free streamlines' S_J at the edge of the jet (see Fig. 2). All of the φ^*-streamlines *cut across* S_J within a distance $\sim\mathscr{O}(d)$ from the aperture. The flow speed on the jet boundary is constant and equal to $U_\sigma\equiv U_\sigma(t)=$ the asymptotic jet velocity predicted by free-streamline theory (Birkhoff and Zarantonello, 1957; Gurevich, 1965).

This simple model can be used to evaluate approximately the final integral of (2.9). The free-streamline jet boundary S_J is spanned by circular vortex lines with centres on the x_3-axis and with $\boldsymbol{\omega}=U_\sigma\delta(s_\perp)\hat{\boldsymbol{\theta}}$, where $s_\perp$ is distance measured in the direction of the outward normal from S_J and $\hat{\boldsymbol{\theta}}$ is a unit azimuthal vector (directed anticlockwise when viewed in

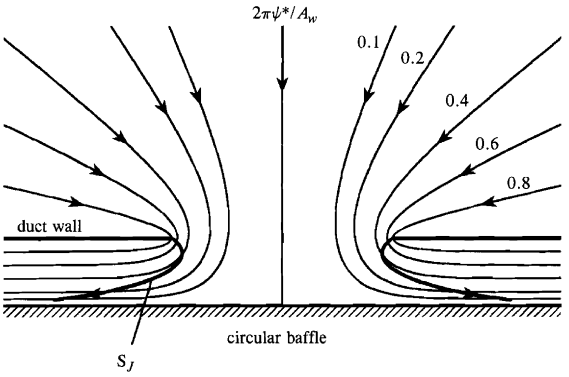

Fig. 2. Illustrating the intersection of the streamline pattern $\psi^* =$ constant of the potential function φ^* with the jet shear layer when $d/R_w = 0.6$.

the direction of increasing x_3); the vorticity convection velocity $\mathbf{v} = \frac{1}{2}U_\sigma \mathbf{t}$, where $\mathbf{t}$ is a unit vector tangential to S_J in flow direction. Hence, because $\hat{\boldsymbol{\theta}} \wedge \mathbf{t}$ is the unit normal on S_J directed outwards from the jet, the spatial component of the final integral of (2.9) becomes

$$\int (\boldsymbol{\omega} \wedge \mathbf{v} \cdot \nabla\varphi^*)(\mathbf{y},\tau)\,\mathrm{d}^3\mathbf{y} = \frac{1}{2}U_\sigma^2(\tau)\oint_{S_J}\left(\frac{\partial\varphi^*}{\partial s_\perp}\right)_{s_\perp=0}\mathrm{d}S \approx \frac{\mathscr{A}_w}{2}U_\sigma^2(\tau). \tag{2.10}$$

Therefore Eq. (2.9) reduces to

$$p_s\left(t-\frac{|x_1|}{c_0}\right) = -\frac{c_0\mathscr{A}_w}{2\mathscr{A}\mathscr{L}}\int_{-\infty}^{[t]}\left(p_I - \frac{1}{2}\rho_0 U_\sigma^2\right)(\tau)\exp\left[-\frac{c_0\mathscr{A}_w}{2\mathscr{A}\mathscr{L}}([t]-\tau)\right]\mathrm{d}\tau. \tag{2.11}$$

To calculate U_σ we introduce the *outflow* velocity $V(t)$ averaged over the cross-section of the aperture, and the acoustic particle velocity

$$U_s(t-|x_1|/c_0) = \frac{p_s(t-|x_1|/c_0)}{\rho_0 c_0} \tag{2.12}$$

of the scattered wave in the duct. Continuity of volume flux at low frequencies requires that

$$U_s(t) = -\frac{\mathscr{A}_w V(t)}{2\mathscr{A}}, \quad U_\sigma(t) = \frac{V(t)}{\sigma}, \tag{2.13}$$

where σ is the effective aperture *discharge coefficient* (or jet 'contraction ratio'). A differential equation satisfied by $V(t)$ is now obtained by formally taking the limit $|x_1| \to 0$ in (2.11) and (2.12) and differentiating (2.11) with respect to time, to find

$$\mathscr{L}\frac{\mathrm{d}V}{\mathrm{d}t} + \frac{\mathscr{A}_w c_0 V}{2\mathscr{A}} + \frac{V^2}{2\sigma^2} = \frac{p_I(t)}{\rho_0}. \tag{2.14}$$

This equation determines the volume flux through the baffled aperture when forced by the incident pressure p_I. Its solution and the second of Eqs. (2.13) determine the nonlinear vortex source term in the representation (2.11) of the sound radiated in the duct from the aperture. However, this sound is more easily calculated directly in terms of $V(t)$ by using Eq. (2.12) and the first of Eqs. (2.13).

2.4. Cummings's equation

Eq. (2.14) generalises Cummings's (1984, 1986) equation (Howe, 1998a) used to study the transmission of sound through an orifice in a large plane wall. The length $\mathscr{L}$ is the effective length of a slug of fluid (of cross-sectional area $\mathscr{A}_w$) set in motion through the aperture. The particular representation (2.8) can be regarded as the sum of three parts: (a) a length $\ell_1 = (\pi/4)R_w$ for the fluid set in motion in the duct (the same as on one side of an aperture in an infinite plane wall); (b) the wall thickness ℓ_w; and (c) the remaining effective length $\mathscr{L} - (\ell_1 + \ell_w)$ of fluid on the outer side of the aperture. Cummings (1984, 1986) points out that this decomposition is valid only for irrotational flow. When the outflow forms a jet the inertia of the fluid determined by the lengths (b) and (c) is progressively eliminated because the

motion in the outflow is ultimately confined only to the jet. To account for this Cummings replaces $\mathscr{L}$ in (2.14) by

$$\bar{\mathscr{L}} = \ell_1 + \frac{\mathscr{L} - \ell_1}{\left[1 + \frac{1}{3}\left(\frac{L_J}{2R_w}\right)^{1.585}\right]}, \tag{2.15}$$

in which L_J is the effective length of the jet, defined by

$$L_J(\tau) = \int_0^\tau |V(t')|\,\mathrm{d}t', \tag{2.16}$$

where τ is measured from the instant at which the mean velocity $V(t)$ last changed sign. The numerical coefficients in (2.15) were validated by experiment. The influence of the functional form of $\bar{\mathscr{L}}$ on the acoustic properties of the aperture is actually limited in practice to the initial transient form of the induced aperture flow, the subsequent behaviour tends to be dominated by the nonlinear term on the left of (2.14). We shall therefore assume that (2.15) is applicable also to the baffled aperture with the wall jet.

The discussion thus far has been implicitly for the case $V(t)>0$ where the jet is directed *out* of the duct. When $V<0$ Eq. (2.14) remains valid provided V^2 is replaced by $V|V|$. For a free jet Cummings found by experiment that the effective value of contraction ratio σ could be taken to be constant and equal to 0.75, which is larger than the steady state limit 0.62 for a continuous jet. We shall use this value when the jet is directed into the duct. During outflow, however, when the jet impinges on the baffle at a standoff distance d, we use the following formula derived in Appendix B

$$\sigma = 0.75\,\mathrm{erf}\left(1.43\frac{d}{R_w}\right), \tag{2.17}$$

where $\mathrm{erf}(x) = (2/\sqrt{\pi})\int_0^x \mathrm{e}^{-\xi^2}\,\mathrm{d}\xi$ is the error function, so that $\sigma\sim 0.75$ when $d \gg R_w$.

In summary, the following revised form of the aperture velocity equation (2.14) will be used

$$\bar{\mathscr{L}}\frac{\mathrm{d}V}{\mathrm{d}t} + \frac{\mathscr{A}_w c_0 V}{2\mathscr{A}} + \frac{V|V|}{2\sigma^2} = \frac{p_I(t)}{\rho_0}, \tag{2.18}$$

where

$$\bar{\mathscr{L}} = \begin{cases} \mathscr{L} - (\ell_1 + \ell_w) + (\ell_1 + \ell_w)\Big/\left[1 + \frac{1}{3}\left(\frac{L_J}{2R_w}\right)^{1.585}\right] & \text{for } V<0, \\ \ell_1 + (\mathscr{L} - \ell_1)\Big/\left[1 + \frac{1}{3}\left(\frac{L_J}{2R_w}\right)^{1.585}\right] & \text{for } V>0, \end{cases} \tag{2.19}$$

$$\sigma = \begin{cases} 0.75 & \text{for } V<0, \\ 0.75\,\mathrm{erf}\left(1.43\frac{d}{R_w}\right) & \text{for } V>0 \end{cases} \tag{2.20}$$

and L_J is defined as in (2.16).

3. Incident acoustic compression wave

Consider first an incident wave in the form of a compression wave $p_I(t + x/c_0)$ of amplitude p_c defined by

$$p_I = \frac{p_c}{2}\left\{1 + \mathrm{erf}\left(\frac{c_0}{\delta}\left[t + \frac{x_1}{c_0}\right]\right)\right\}, \tag{3.1}$$

where $\mathrm{erf}(\cdot)$ is the error function introduced in Section 2.4. The length 2δ defines the thickness of the wavefront, which is required to be large compared to the diameter of the wall aperture ($\delta \gg R_w$), so that the incident pressure may be assumed to be uniform over the inner face of the aperture.

Eqs. (2.12) and (2.13) supply the net acoustic pressure in the duct in the form

$$p = p_I\left(t + \frac{x_1}{c_0}\right) - \frac{\rho_0 c_0 \mathscr{A}_w}{2\mathscr{A}} V\left(t - \frac{|x_1|}{c_0}\right), \tag{3.2}$$

where $V(t)$ is the solution of the system of Eqs. (2.16)–(2.20). These equations are to be solved subject to the initial conditions

$$V = 0, \quad L_J = 0, \quad t \to -\infty. \tag{3.3}$$

To examine the effect of varying standoff distance d/R_w we consider an incident wave amplitude $p_c = 2.5\,\mathrm{kPa}$ and wavefront thickness $2\delta = 4R \equiv 4\sqrt{\mathscr{A}/\pi}$, where R is the radius of the circle whose area is the same as cross-sectional area of the duct. A wave of this amplitude is typical of that of the compression wave generated when a high-speed train enters a uniform tunnel of semi-circular cross-section of radius R (Howe et al., 2006).

For the purposes of illustration we take

$$\frac{D}{R} = 1, \quad \frac{\mathscr{A}_w}{\mathscr{A}} = 0.1, \quad \ell_w = 0, \tag{3.4}$$

so that $R_w/R = 0.316$ and the wave thickness $2\delta = 4D$.

Profiles of the calculated wave (3.2) transmitted past the aperture (into the region $x_1 < 0$) are plotted as the solid line curves in Fig. 3 for values of the relative baffle standoff distance d/R_w given in Table 1.

The aperture has no effect when $d/R_w = 0$, so that the transmitted and incident waves are the same. Pressure relaxation occurs at the aperture when $d/R_w > 0$. In all cases, however, the shape of the initial pressure rise is essentially unaffected by the initial stages of jet formation in the aperture. For this problem the jet is always directed outwards from the duct ($V > 0$). The jet inertia acts as an acoustic 'block' at the aperture, and is most significant when d/R_w is small: the corresponding value of the contraction ratio σ is displayed in Table 1; small values of σ increase the influence of the nonlinear inertia term in Eq. (2.18). The enhancement of nonlinearity produced by jet impingement becomes unimportant for $d > 2R_w$, when σ assumes its free field value of 0.75. The results are only weakly dependent on the 'slug length' $\mathscr{L}$, which also depends on d/R_w.

The pressure to the rear of the transmitted wavefront relaxes to a constant value determined by the following steady state solution of Eq. (2.18), obtained by discarding the first term on the left-hand side:

$$p(t + x_1/c_0) \sim p_c - \frac{\rho_0 c_0^2 \sigma^2}{4}\left(\frac{\mathscr{A}_w}{\mathscr{A}}\right)^2 \left\{\sqrt{1 + \left(\frac{\mathscr{A}}{\mathscr{A}_w}\right)^2 \frac{8p_c}{\rho_0 c_0^2 \sigma^2}} - 1\right\}, \quad \frac{c_0[t]}{R} \gg 1. \tag{3.5}$$

Table 1
The contraction ratio σ and slug length $\mathscr{L}$ (for conditions (3.4)) when $V(t) > 0$.

d/R_w	0	0.25	0.5	1.0	2.0
σ	0	0.29	0.52	0.72	0.75
$\mathscr{L}/R_w$	∞	3.3	2.2	1.6	1.5

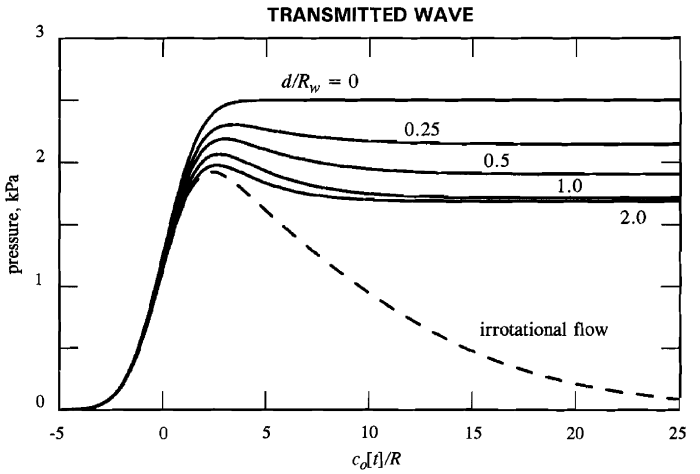

Fig. 3. Transmission of the compression wave (3.1) past the baffled aperture for different values of d/R_w for $p_c = 2.5\,\mathrm{kPa}$, $\delta = 2R$ and conditions (3.4), where $[t] = t + x_1/c_0$.

The broken line curve in Fig. 3 is the irrotational approximation to the transmitted wave when the baffle plate is absent. The velocity $V(t)$ is calculated by putting $\sigma = \infty$ in (2.18) and $\tilde{\mathscr{P}} = 2 \times (\pi/4)R_w$, the value appropriate for a circular aperture in a plane wall. High frequency components of an incident wave are transmitted past the aperture, but the low frequency tail of the wave cannot pass the aperture in this ideal, irrotational limit because of the formation of an expansion wave of amplitude $-p_c$ that radiates within the duct in both directions from the aperture.

4. Compression wave generated by a train

4.1. Formulation

Application of the theory is now made to the model scale experiment depicted in Fig. 4, involving a *circular* cylindrical, thin-walled tunnel of radius R and cross-sectional area $\mathscr{A} = \pi R^2$ containing a baffled, circular 'window' whose centre is distance ℓ_h from the tunnel portal. Any influence of the change in shape of the duct cross-section, from rectangular to circular, should be small provided the window area is small relative to the duct cross-sectional area. The theory will be compared with experiment in Section 5, where the baffle is taken to represent the influence of the wall of a 'cutting' adjacent to the tunnel. It is convenient to introduce a new coordinate system $\mathbf{x} = (x, y, z)$ (the suffix notation is abandoned to avoid confusion with the earlier coordinates used in Sections 2 and 3) with the origin O on the cylinder axis in the entrance plane; the x-axis is coaxial with the cylinder and is directed out of the tunnel.

An axisymmetric model train enters the tunnel from $x > 0$ and travels in the negative x-direction at constant speed U. The axes of the train and tunnel coincide. It is required to determine the influence of the baffled window on the compression wave generated by the train. The initial form of the wavefront cannot depend on the length of the tunnel, which is therefore assumed to extend to $x = -\infty$. Similarly, for the purpose of calculating the compression wave it is convenient to assume that the length of the train greatly exceeds the 'nose length' L indicated in the figure, beyond which the circular cross-section of the train is taken to be uniform with radius h and area $\mathscr{A}_0 = \pi h^2$.

4.2. Compression wave when the window is absent

The influence of the window on the compression wave is determined by a modified form of Eqs. (2.16)–(2.20), in which the incident wave p_I corresponds to the pressure wave produced by the train in the absence of the window.

The main pressure rise p_e across the wavefront is generated over a time $\sim 2R/U$ during which the centroid of the train nose may be assumed to enter the tunnel. Reynolds and Nusselt numbers based on tunnel radius are typically of order 10^5 in the experiments (and $\sim 10^7$ at full scale), which implies that the initial form of p_e can be found by neglecting viscous diffusion and heat transfer. At later times flow separation from the train (from S in Fig. 4(a)) produces a wake that generates a very low frequency component p_w of the pressure in the form of an extensive, linearly growing 'tail' to the rear of the wavefront (the growth being proportional to the retarded length of the train within the tunnel). The

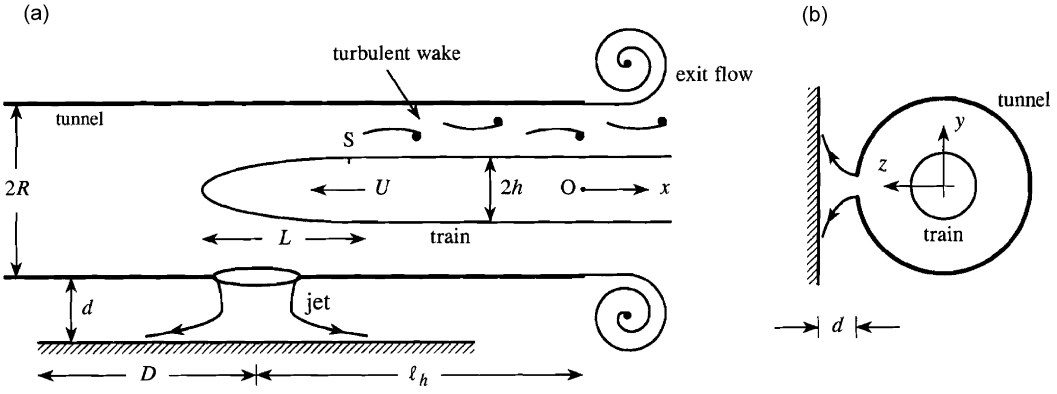

Fig. 4. Circular cylindrical tunnel of radius R with a baffled window of radius $R_w = \sqrt{\ell_x \ell_y/\pi}$ with its geometric centre at $x = -\ell_h,\ y = 0,\ z = R$. An axisymmetric train enters the tunnel portal at $x = 0$ travelling along the centreline of the tunnel at constant speed U: (a) view from above; (b) view into the tunnel.

pressure wave *ahead* of the train can therefore be cast in the form

$$p = p_e + p_w. \tag{4.1}$$

It was shown by Howe (1999) and confirmed by experiments reported by Howe et al. (2000) that an excellent approximation to the component p_e at positions x (<0) within the tunnel ahead of the train is given by

$$p_e(x,t) \approx \frac{\rho_0 U^2}{\mathscr{A}(1-M^2)}\left(1+\frac{\mathscr{A}_0}{\mathscr{A}}\right)\int_{-\infty}^{\infty}\frac{\partial \mathscr{A}_T}{\partial x'}(x'+U[t])\frac{\partial \varphi_E^*}{\partial x'}(x',0,0)\,\mathrm{d}x', \tag{4.2}$$

where $M = U/c_0$ is the train Mach number, $\mathscr{A}_0/\mathscr{A}$ is the 'blockage', $\mathscr{A}_T(s)$ is the cross-sectional area of the train at an axial distance s from the front of the nose, $[t] = t + (x-\ell_E)/c_0$ is the effective retarded time, and ℓ_E is the acoustic 'end correction' of the tunnel portal [$\sim 0.61R$ for an unflanged circular cylindrical portal; see Rayleigh (1926) and Howe (1998a)]. The function $\varphi_E^*(\mathbf{x}) \equiv \varphi_E^*(r,x)$ (where $r = \sqrt{y^2+z^2}$) is that solution of Laplace's equation that represents the potential of incompressible flow *out* of the tunnel portal having unit speed within the tunnel. The following formula is applicable for a thin-walled tunnel in the form of an unflanged, circular cylinder (Howe, 1998b):

$$\left.\begin{aligned}\frac{\partial \varphi_E^*}{\partial x}(r,x) &= \frac{1}{2} - \frac{1}{2\pi}\int_0^\infty \mathrm{I}_0\left(\lambda\frac{r}{R}\right)\sqrt{\frac{2\mathrm{K}_1(\lambda)}{\mathrm{I}_1(\lambda)}}\sin\left(\lambda\left[\frac{x}{R}+\mathscr{F}(\lambda)\right]\right)\mathrm{d}\lambda, \quad r<R,\\ \mathscr{F}(\lambda) &= \frac{1}{\pi}\int_0^\infty \frac{\ln[\mathrm{K}_1(\mu)\mathrm{I}_1(\mu)/\mathrm{K}_1(\lambda)\mathrm{I}_1(\lambda)]}{\mu^2-\lambda^2}\mathrm{d}\mu,\end{aligned}\right\} \tag{4.3}$$

where I_0, I_1, K_1 are modified Bessel functions.

The integrand of (4.2) is nonzero only at the retarded positions of the nose and tail of the train where $\partial \mathscr{A}_T/\partial x' \neq 0$. Model scale tests have confirmed the validity of (4.2) for $\mathscr{A}_0/\mathscr{A} \leqslant 0.2$ and $M < 0.35$.

In the experiments discussed in Section 5 the interior tunnel radius R, the wall thickness ℓ_w, and the window centroid $x = -\ell_h$ have the following respective values:

$$R = 50\,\mathrm{mm}, \quad \ell_w = 0.1R, \quad \ell_h = 10R. \tag{4.4}$$

The experimental train has an ellipsoidal nose defined by

$$\left.\begin{aligned} r &= h\sqrt{\frac{x}{L}\left(2-\frac{x}{L}\right)}, \quad 0<x<L \ \left(r=\sqrt{y^2+z^2}\right),\\ h &= 22.35\,\mathrm{mm}, \quad L = 67.05\,\mathrm{mm},\end{aligned}\right\} \tag{4.5}$$

so that the blockage $\mathscr{A}_0/\mathscr{A} = 0.2$.

Eq. (4.2) has been used to calculate the pressure p_e depicted in Fig. 5 when the train enters the tunnel at $U = 300\,\mathrm{km/h}$. The retarded time is taken in the nondimensional form $U[t]/R$, where $[t] = t + (x-\ell_E)/c_0$, and the nose of the train is assumed to pierce the tunnel entrance plane at $t = 0$. The pressure p_e rises rapidly across the wavefront during a time $\sim 2R/U$ by an amount

$$\frac{\rho_0 U^2}{(1-M^2)}\frac{\mathscr{A}_0}{\mathscr{A}}\left(1+\frac{\mathscr{A}_0}{\mathscr{A}}\right) \sim 2.18\,\mathrm{kPa}.$$

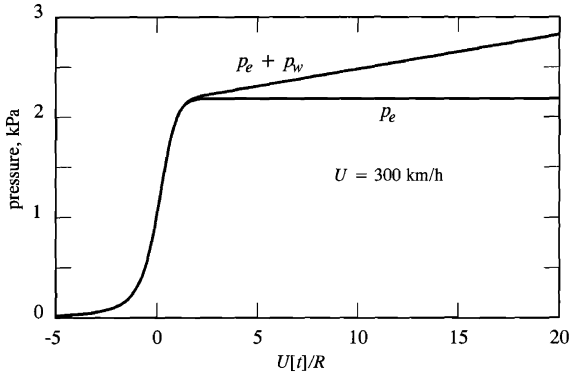

Fig. 5. The pressure waves p_e and $p_e + p_w$ generated at the tunnel portal in the model scale tunnel of radius $R = 50\,\mathrm{mm}$ by the axisymmetric train with nose profile (4.5) when $U = 300\,\mathrm{km/h}$ and friction factor $\mu = 0.053$.

The actual thickness of the wavefront $\sim 2R/M = 8R$, which is large compared to the tunnel diameter and much larger than a typical window.

The pressure p_w produced by the wake can be calculated using the following formula that has been validated against experiment by Howe and Iida (2003):

$$p_w(x,t) \approx \frac{2\pi\mu^2\rho_0 U^2}{\mathscr{A}(\mathscr{A}-\mathscr{A}_0)^2}\frac{(U[t]-L)_+}{(1-M^2)}\left[R\mathscr{A}_0^2\left(1-\frac{M\mathscr{A}}{(\mathscr{A}-\mathscr{A}_0)}+\frac{M^2\mathscr{A}(2\mathscr{A}-\mathscr{A}_0)}{2(\mathscr{A}-\mathscr{A}_0)^2}\right)^2\right.$$
$$\left.+h\mathscr{A}^2\left(1-\frac{M\mathscr{A}_0}{(\mathscr{A}-\mathscr{A}_0)}+\frac{M^2\mathscr{A}_0(2\mathscr{A}-\mathscr{A}_0)}{2(\mathscr{A}-\mathscr{A}_0)^2}\right)^2\right], \tag{4.6}$$

where $(x)_+ = x, 0$ according as $x \gtrless 0$. This pressure wave increases linearly with the retarded distance $U[t]-\mathscr{L}$ of the separation point S on the train from the tunnel entrance. The coefficient μ is a turbulence friction factor dependent on the train Reynolds number and the blockage $\mathscr{A}_0/\mathscr{A}$. Howe and Iida (2003) found that $\mu \approx 0.053$ for model scale experiments of the type to be considered, and this value has been used to plot in Fig. 5 the overall compression wave $p_e + p_w$ when $U = 300\,\mathrm{km/h}$.

4.3. Calculation of p_I

The air flow through the baffled window at $x = -\ell_h$ (Fig. 4(a)) is driven by the incident pressure p_I of Eq. (2.18). If the nose of the train enters the tunnel at time $t = 0$ the incident wave must coincide with the pressure $p_e + p_w$ prior to the arrival of the train at the window at $t \sim \ell_h/U$. The wave reaches the window at $t \sim \ell_h/c_0$, so that

$$p_I = p_e(-\ell_h,t) + p_w(-\ell_h,t), \qquad t < \frac{\ell_h}{U}. \tag{4.7}$$

The pressure p_I applied to the window decreases rapidly over a time of order L/U as the nose passes the window by an amount equal to the maximum pressure

$$\frac{\rho_0 U^2}{(1-M^2)}\frac{\mathscr{A}_0}{\mathscr{A}}\left(1+\frac{\mathscr{A}_0}{\mathscr{A}}\right)$$

attained by p_e (Fig. 5). The pressure decrease as a function of time is determined to a good approximation by calculating the 'near field' pressure generated on the tunnel wall by a distribution of volume sources on the nose that represent the displacement of air by the advancing train [see Howe (2005) for details]. The actual contribution of p_e to p_I for *all* times is then obtained by replacing $p_e(-\ell_h,t)$ in (4.7) by

$$p_e(-\ell_h,t)\left\{1-\int_{-\infty}^{\infty}\frac{\mathscr{A}_\mathrm{T}(x')}{\mathscr{A}_0}\Psi(Ut-\ell_h-x')\,\mathrm{d}x'\right\}, \tag{4.8}$$

where the nonnegative function

$$\Psi(x) = \frac{1}{2\pi R\sqrt{1-M^2}}\int_0^\infty \frac{\lambda}{\mathrm{I}_1(\lambda)}\cos\left(\frac{\lambda x}{R\sqrt{1-M^2}}\right)\mathrm{d}\lambda \tag{4.9}$$

resembles a 'broadened' δ-function of width $\sim 4R$ that peaks at $x = 0$ and satisfies $\int_{-\infty}^{\infty}\Psi(x)\,\mathrm{d}x = 1$.

The integral in (4.8) vanishes until the train nose approaches the window at $t \sim \ell_h/U$; after the nose has passed the window ($t > (\ell_h + L)/U$) the integral rapidly increases to 1, and the pressure represented by (4.8) drops to zero. Immediately after this, all that remains of the incident pressure (4.7) is the frictional contribution $p_w(-\ell_h,t)$, which must then be equal to its value at $t = (\ell_h + L)/U$ and remain equal to this until the tail of the train enters the tunnel, because the linear pressure rise produced by the wake between the window and the tunnel entrance is constant until the tail enters.

Thus, instead of the representation (4.7), the pressure $p_I(t)$ incident on the baffled window, produced by the train when the presence of the window is ignored, should be taken in the form

$$p_I(t) = \begin{cases} p_e(-\ell_h,t)\left\{1-\int_{-\infty}^{\infty}\frac{\mathscr{A}_\mathrm{T}(x')\Psi(Ut-\ell_h-x')}{\mathscr{A}_0}\mathrm{d}x'\right\} + p_w(-\ell_h,t), & t < (\ell_h+L)/U, \\ p_e(-\ell_h,t)\left\{1-\int_{-\infty}^{\infty}\frac{\mathscr{A}_\mathrm{T}(x')\Psi(Ut-\ell_h-x')}{\mathscr{A}_0}\mathrm{d}x'\right\} + p_w(-\ell_h,(\ell_h+L)/U), & t > (\ell_h+L)/U. \end{cases} \tag{4.10}$$

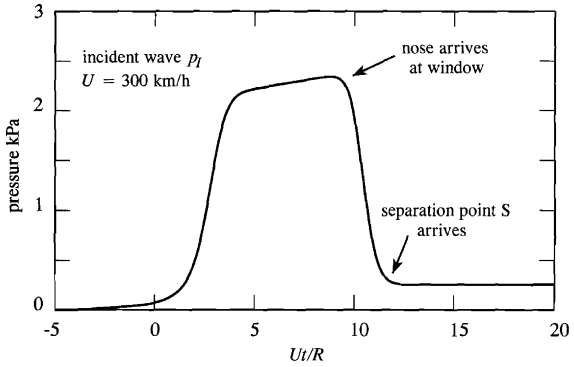

Fig. 6. Variation of the incident pressure $p_I(t)$ on a window whose centroid is at $x=-\ell_h=-10R$ in the model scale tunnel of radius $R=50\,\mathrm{mm}$ when the axisymmetric train with nose profile (4.5) enters the tunnel at $U=300\,\mathrm{km/h}$ and when the friction factor $\mu=0.053$.

The variation of $p_I(t)$ with time predicted by this formula is illustrated in Fig. 6 for the train and tunnel considered previously in Fig. 5 when the window is centred at $x=-\ell_h=-10R$.

4.4. The compression wave transmitted past the window

When the tunnel portal is ignored, the unsteady flow out of the baffled window at speed $V(t)$ generates the plane pressure waves

$$p_s\left(t\mp\frac{(x+\ell_h)}{c_0}\right),\quad x\gtrless-\ell_h\ \text{ where } p_s(t)=-\frac{\rho_0c_0\mathscr{A}_w}{2\mathscr{A}}\,V(t). \tag{4.11}$$

The component $p_s(t-(x+\ell_h)/c_0)$ is reflected at the tunnel portal with sign reversal. Because the characteristic wavelength is large compared to the tunnel diameter the reflection at the open end actually appears to occur at $x=\ell_E$, so that the reflected wave is

$$-p_s\left(t+\frac{[x-(\ell_h+2\ell_E)]}{c_0}\right),\quad x<0, \tag{4.12}$$

which may be interpreted as the field produced by a 'negative' image window at $x=\ell_h+2\ell_E$. This reflected pressure evaluated at $x=-\ell_h$ must be introduced as an additional forcing pressure on the right-hand side of the aperture velocity equation (2.18), which may now be expressed in the following modified form:

$$\begin{aligned}\tilde{\mathscr{L}}\frac{\mathrm{d}V}{\mathrm{d}t}&=\frac{p_I(t)}{\rho_0}+p_s(t)-p_s\left(t-\frac{2(\ell_h+\ell_E)}{c_0}\right)-\frac{V(t)|V(t)|}{2\sigma^2}\\&\equiv\frac{p_I(t)}{\rho_0}-\frac{\mathscr{A}_wc_0V(t)}{2\mathscr{A}}+\frac{\mathscr{A}_wc_0V\left(t-\dfrac{2(\ell_h+\ell_E)}{c_0}\right)}{2\mathscr{A}}-\frac{V(t)|V(t)|}{2\sigma^2},\end{aligned} \tag{4.13}$$

where $p_I(t)$ is given by (4.10) and σ is defined as in (2.20).

In addition, however, the definition of the effective length $\tilde{\mathscr{L}}(t)$ must also be adjusted, because in Section 2 the tunnel wall and the baffle panel were assumed to be parallel and distance d apart, which differs from the experimental arrangement illustrated schematically in Fig. 4, where d is now the shortest distance between the window and the baffle. This change actually affects only the contribution to $\tilde{\mathscr{L}}(t)$ from the region *exterior* to the window. Because this tends to be 'blown away' very rapidly during the initial stages of jet formation, and the exterior region is now approximately acoustically 'open', we shall assume that the exterior contribution to $\tilde{\mathscr{L}}(t)$ is $\ell_1=(\pi/4)R_w$, the same as for the opening on the side within the tunnel. This implies that the definition (2.19) can be reduced to

$$\tilde{\mathscr{L}}(t)=\ell_1+\frac{\ell_1+\ell_w}{\left[1+\dfrac{1}{3}\left(\dfrac{L_J}{2R_w}\right)^{1.585}\right]},\quad \ell_1=\frac{\pi}{4}R_w,\quad V(t)\gtrless0. \tag{4.14}$$

The causal solution of Eq. (4.13) is required, subject to the initial conditions $V, L_J = 0$ for t large and negative. The solution is used to compute the compression wave pressure $p(x,t)$ radiated beyond the window into the tunnel ahead of the train by means of

$$p(x,t) = p_e(x,t) + p_w(x,t) + p_s\left(t + \frac{(x+\ell_h)}{c_0}\right) - p_s\left(t + \frac{[x-(\ell_h+2\ell_E)]}{c_0}\right), \tag{4.15}$$

where $p_s(t) = -\rho_0 c_0 V(t)\mathscr{A}_w/\mathscr{A}$.

5. Comparison with experiment

Predictions of Eq. (4.15) are now compared with model scale experiments performed at train speeds $U\sim 300-400$ km/h at the Railway Technical Research Institute in Tokyo. The experimental train and tunnel, and the procedures for measuring the pressure and train speed are the same as those used and described in detail by Howe et al. (2003a). The tunnel consisted of a 6.5 m long horizontal, hard walled, unflanged circular cylindrical pipe of inner diameter $2R = 100$ mm. An adjustable *rectangular* window of dimensions $\ell_x \times \ell_y$, respectively, in the x and y directions was situated in the *upper* wall of the tunnel with its centroid vertically above the tunnel axis at distance $\ell_h = 10R = 0.5$ m from the entrance plane. The tunnel wall thickness at the window was $\ell_w = 0.1R$. The original apparatus was modified by the addition of a rigid, square and horizontal aluminium baffle panel with sides of length 0.5 m fixed above the tunnel and centred on the window. The face of the panel wetted by the jet was at $z = R + d$. The photograph (Fig. 7) shows the arrangement when $d = 80$ mm.

Measurements were made for cases involving either a 'small' or a 'long slit' window with the specifications given in Table 2.

A model axisymmetric train with an ellipsoidal nose profile defined as in Eq. (4.5) was projected into the tunnel by means of a three-stage friction drive involving three pairs of rotating wheels; the train was guided along a 5 mm diameter taut steel wire stretched along the tunnel axis and passing smoothly through a cylindrical bore hole along the train axis. The compression wave pressure was measured using a flush mounted wall sensor in the tunnel 1.5 m from the tunnel entrance plane ($x = -1.5$ m), with an overall error estimated to be between 2% and 3%. Estimates were also made of the likely errors produced by wave reflection from the laboratory walls, ceiling and floor. Image sources in the floor (about 1 m below the tunnel) were considered to be the most important source of reflections. However, simple estimates of the magnitude of reflected sound at the tunnel mouth indicated that this could modify pressures within the tunnel by no more than about 0.1% of the total pressure rise across the compression wave front.

The pressure gradient $(\mathrm{d}p/\mathrm{d}t)$ was calculated using a simple central difference scheme after high frequency components (>2 kHz for $U = 300$ km/h and >2.5 kHz for $U = 400$ km/h) of the measured pressure were removed using a fast Fourier transform algorithm. The temperature and atmospheric pressure were measured for each run and later used to calculate the mean density of air from the equation of state of an ideal gas.

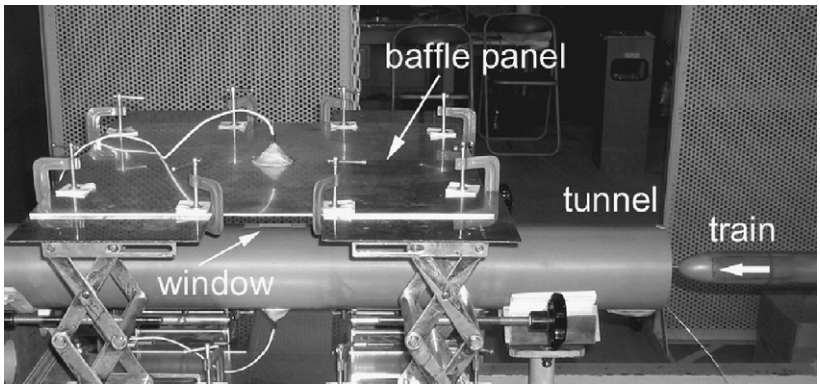

Fig. 7. Side view of the experimental model scale configuration, involving a circular cylindrical tunnel and an adjacent square baffle panel.

Table 2
Window dimensions.

Window	ℓ_x (mm)	ℓ_y (mm)
Small	20 (0.4R)	20 (0.4R)
Long slit	80 (1.6R)	20 (0.4R)

5.1. Baseline validation of the prediction equations

We first verify that the test procedure conforms with the known general agreement between theory and experiment (Howe et al., 2006) for the baseline cases

(a) No window: $U = 298\,\mathrm{km/h}$, $\rho_0 = 1.22\,\mathrm{kg/m^3}$.
(b) Small window, no baffle: $U = 300\,\mathrm{km/h}$, $\rho_0 = 1.19\,\mathrm{kg/m^3}$, $\sigma = 0.75$.

Fig. 8 displays the measured compression wave pressure p ($\triangle\ \triangle\ \triangle$) and the 'pressure gradient' $\partial p/\partial t$ (•••) produced by the model train (4.5). The variation of $\partial p/\partial t$ is of interest because it determines the subjective impact of the wave (Maeda, 2002). In all cases the time origin is adjusted to coincide with the instant at which the train nose begins to cross the entrance plane of the tunnel. The solid curves in the figure are the predictions of (4.15). The theory is strictly applicable only to circular windows; it has therefore been assumed in case (b) that the action of the square window of dimensions $\ell_x = \ell_y = 20\,\mathrm{mm}$ is equivalent to that of a circular window of equal area, with $R_w = \sqrt{\ell_x \ell_y/\pi} = 11.28\,\mathrm{mm}$.

The fine details of the predictions at later times are influenced significantly by the wake-generated component p_w of the pressure, and therefore by the value assigned to the friction factor μ of Eq. (4.6). Model scale tests reported by Howe and Iida (2003) indicate that $\mu \sim 0.053$ yields results that agree well with experiment at later times (for $U[t]/R > 12$, say). However, there is no Reynolds number similarity between full and model scale, so that both the present theoretical predictions and model scale tests should not necessarily be expected to yield accurate predictions at full scale at large times. The drag is also influenced by surface roughness, which is usually unimportant at model scale, but may cause p_w to make a substantially larger relative contribution at full scale, when irregular surface structures are present, particularly beneath the train. In what follows the value of the friction factor has been modified where necessary (from $\mu = 0.053$, the new value being indicated on the corresponding graph) to give the best overall agreement between the measured and predicted pressure at large times.

5.2. Small window experiments

Measurements were made with the small window for four different values of the baffle standoff distance d. The train speed was maintained at $U = 300\,\mathrm{km/h}$ in all cases; other relevant parametric values are listed in Table 3, on the basis that the equivalent radius of the window can be taken to be $R_w = 11.28\,\mathrm{mm}$, and where σ is calculated for the outflowing jet using Eq. (2.17).

The graphical comparison of theory and experiment for all of the small window tests are presented in Fig. 9. A careful inspection reveals that although the overall effect of the baffle is small, the close proximity of the baffle to the window in Cases (i) and (ii) leads to a small elevation in the magnitude of the initial pressure rise at the wavefront. The results for Cases (iii) and (iv) are essentially identical to those in Fig. 8(b) for the unbaffled window.

5.3. Long slit window experiments

The long slit window has an equivalent radius $R_w \sim 0.45R$, which is too large for the theory of Section 4 to be strictly applicable. We therefore adopt the procedure successfully used by Howe et al. (2006) to determine the influence on compression wave formation of large *unbaffled* windows, viz. the replacement of the slit window by a distribution along its length of smaller 'subwindows' having the same total area. To do this the long slit window of dimensions $\ell_x = 1.6R$, $\ell_y = 0.4R$ is replaced by four equal subwindows each with $\ell_x = \ell_y = 0.4R$ and equivalent radius $R_w = 0.127R \sim 11.28\,\mathrm{mm}$, equally spaced with centroids at $x = -\ell_{hk}$, $k = 1, 2, 3, 4$, where $\ell_{hk}/R = 9 + 0.4k$.

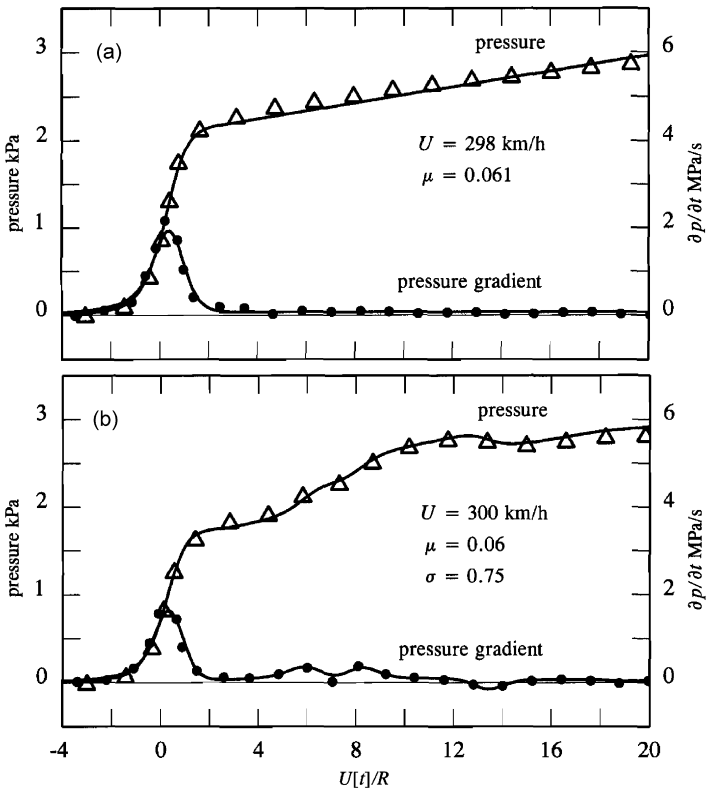

Fig. 8. Measured (△△△, ···) and predicted (——) compression wave pressure and pressure gradient: (a) no window, when $U = 298\,\mathrm{km/h}$ and $\rho_0 = 1.22\,\mathrm{kg/m^3}$; (b) small, unbaffled window at distance $\ell_h = 10R$ from the tunnel portal, when $U = 300\,\mathrm{km/h}$, $\rho_0 = 1.19\,\mathrm{kg/m^3}$, $\sigma = 0.75$. The model scale train defined by (4.5) is projected along the centreline of the tunnel. Measurements are made within the tunnel at a distance of 1.5 m from the entrance plane.

Table 3
Parameter values for the small window; σ is given for the outflowing jet.

Case	d (mm)	d/R_w	σ ($V>0$)	ρ_0 (kg/m^3)
(i)	5.3	0.47	0.494	1.18
(ii)	10.0	0.89	0.696	1.19
(iii)	20.0	1.77	0.750	1.17
(iv)	40.0	3.55	0.750	1.17

Formula (4.15) for the pressure radiated into the tunnel must now be replaced by

$$p(x,t) = p_e(x,t) + p_w(x,t) + \sum_k \left\{ p_{sk}\left(t + \frac{(x+\ell_{hk})}{c_0}\right) - p_{sk}\left(t + \frac{[x-(\ell_{hk}+2\ell_E)]}{c_0}\right)\right\}, \tag{5.1}$$

where p_{sk} is defined for each subwindow of area $\mathscr{A}_w$ as in (4.11), with $V(t)$ replaced by the corresponding window velocity, which will be denoted by $V_k(t)$ for the k th window.

Similarly, Eq. (4.13) must be replaced by four coupled simultaneous equations for the velocity V_k through each of the four subwindows. Because each subwindow is subject to the driving pressure generated by the other subwindows it is

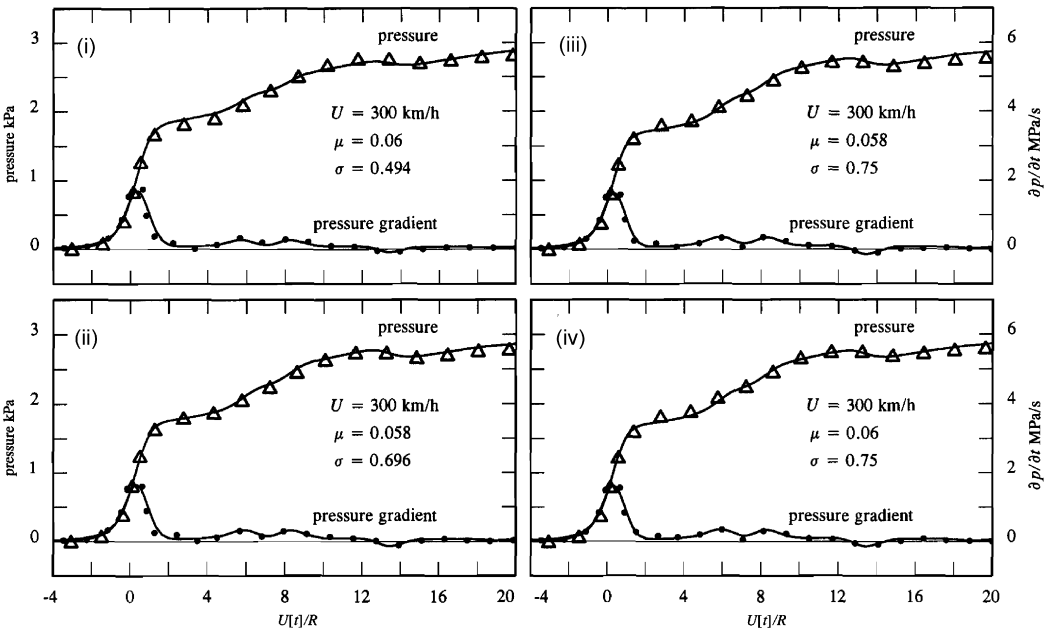

Fig. 9. Measured (△△△, ···) and predicted (——) compression wave pressure and pressure gradient for the small window experiments of Table 3, all at $U = 300\,\mathrm{km/h}$. The model scale train defined by (4.5) is projected along the centreline of the tunnel. Measurements are made within the tunnel at a distance of 1.5 m from the entrance plane.

Table 4
Parameter values for the long slit window; σ is given for the outflowing jet.

Case	d (mm)	d/R_w (subwindow)	σ (subwindow, $V>0$)	ρ_0 (kg/m^3)
(i)	4.9	0.43	0.465	1.19
(ii)	9.9	0.88	0.694	1.19
(iii)	19.9	1.76	0.750	1.20
(iv)	40.0	3.55	0.750	1.20

easily seen that V_k must satisfy

$$\bar{\mathscr{L}}_k \frac{\mathrm{d}V_k}{\mathrm{d}t} = \frac{p_{Ik}(t)}{\rho_0} + \sum_{j=1}^{4}\left\{p_{sj}\left(t - \frac{|\ell_{hk} - \ell_{kj}|}{c_0}\right) - p_{sj}\left(t - \frac{(\ell_{hk} + \ell_{kj} + 2\ell_E)}{c_0}\right)\right\} - \frac{V_k(t)|V_k(t)|}{2\sigma^2}, \tag{5.2}$$

where $\bar{\mathscr{L}}_k$ is defined as in (4.14) with L_J determined by (2.16) with V_k replacing V, and $p_{Ik}(t)$ is the incident pressure (4.10) evaluated at the k th subwindow.

Four tests were made with the long slit window for the baffle standoff distances d and other relevant parameters given in Table 4.

Fig. 10 displays general overall agreement between theory and experiment when the train speed was maintained at $U = 300\,\mathrm{km/h}$. The effect of the near baffle in Case (i) is seen to be marginally more significant than in the corresponding Case (i) for the small window. This is further illustrated in Fig. 11, where the Case (i) measurements and predictions (− − −) for both the small and the long slit windows are compared with the predictions (——) for the corresponding unbaffled window (for which $\sigma = 0.75$). The compression wave amplitude during the initial formation of the wave is significantly underpredicted for the long slit window when no account is taken of the presence of the baffle.

Fig. 12 reveals a corresponding overall agreement between theory and experiment for the long slit cases of Table 4 at the higher speed of $U{\sim}400\,\mathrm{km/h}$.

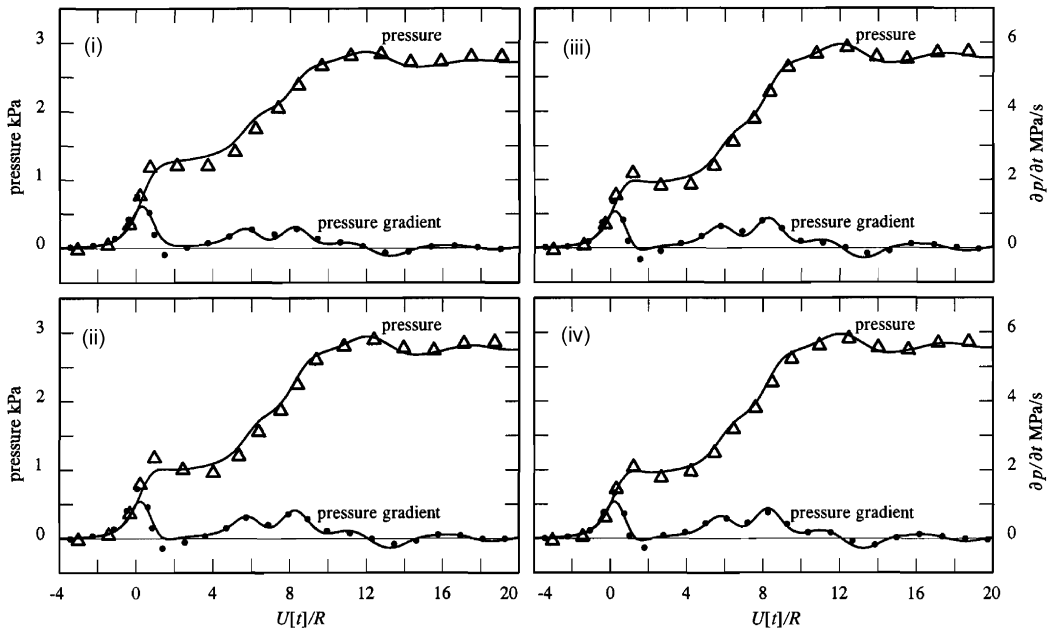

Fig. 10. Measured (△△△, ···) and predicted (——) compression wave pressure and pressure gradient for the long slit window experiments of Table 4, all at $U = 300\,\mathrm{km/h}$ and $\mu = 0.05$. The slit window is divided into four equal square subwindows, each of equivalent radius $R_w = 11.28\,\mathrm{mm}$ with centres at $x/R = -9.4, -9.8, -10.2, -10.6$. The model scale train defined by (4.5) is projected along the centreline of the tunnel. Measurements are made within the tunnel at a distance of 1.5 m from the entrance plane.

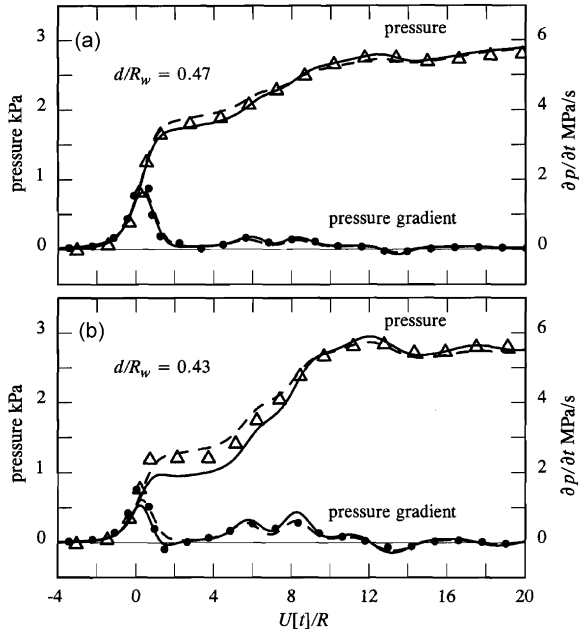

Fig. 11. Measured (△△△, ···) and predicted (– – –) compression wave pressure and pressure gradient for (a) Case (i) of the small window and (b) Case (i) of the long slit window, compared with predictions (——) for the corresponding *unbaffled* window ($\sigma = 0.75$). The slit window is divided into four equal square subwindows, each of equivalent radius $R_w = 11.28\,\mathrm{mm}$ with centres at $x/R = -9.4$, -9.8, -10.2, -10.6. The model scale train defined by (4.5) is projected along the centreline of the tunnel. Measurements are made within the tunnel at a distance of 1.5 m from the entrance plane.

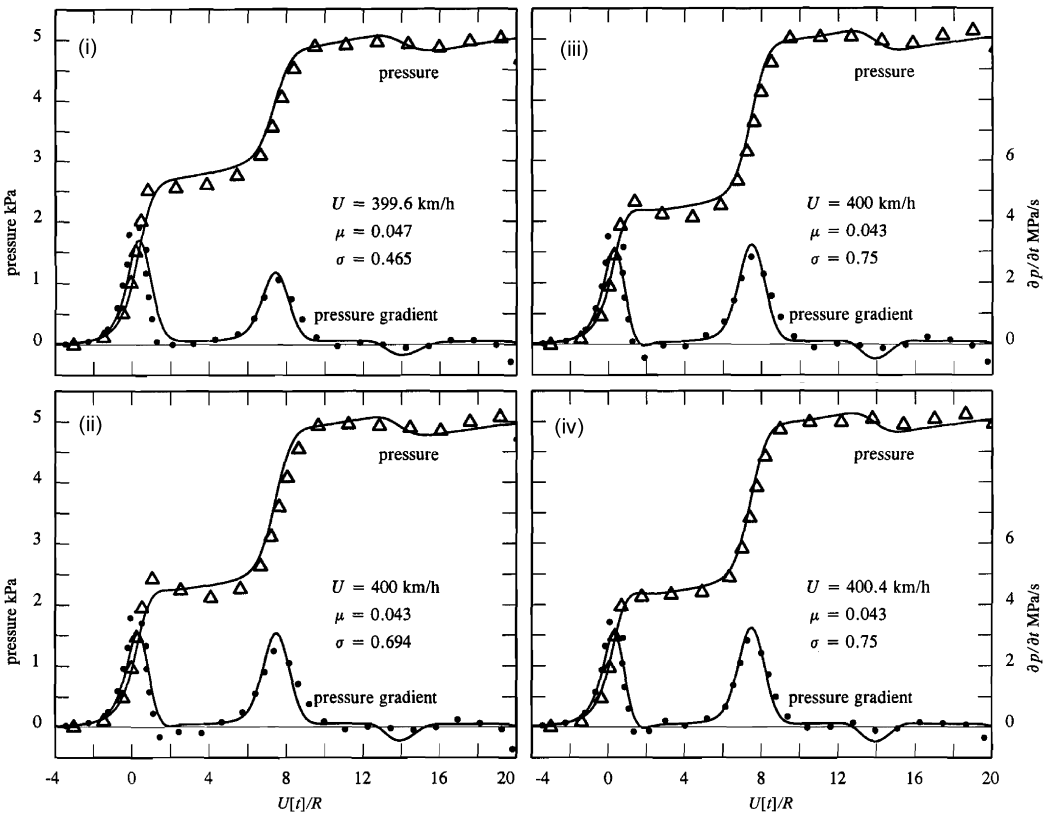

Fig. 12. Measured (△△△, ···) and predicted (——) compression wave pressure and pressure gradient for the long slit window experiments of Table 4, all at $U\sim400$ km/h. The slit window is divided into four equal square subwindows, each of equivalent radius $R_w = 11.28$ mm with centres at $x/R = -9.4, -9.8, -10.2, -10.6$. The model scale train defined by (4.5) is projected along the centreline of the tunnel. Measurements are made within the tunnel at a distance of 1.5 m from the entrance plane.

6. Conclusion

Vorticity produced when fluid is forced through the constriction formed by a baffled wall aperture is responsible for the principal characteristics of the sound generated at the aperture. In the absence of vorticity the aperture typically acts as a 'pressure release' opening (the traditional behaviour of a woodwind finger hole) and predictions based on this model are generally irrelevant in practice except at extremely high frequencies. For the low frequency problems discussed in this paper the whole character of the flow in the aperture and the sound generated depends crucially on the nonlinear 'blocking' of the motion by the vorticity.

An approximate nonlinear equation for the volume flux through the baffled aperture is easily deduced from the theory of vortex sound. It is a generalisation of Cummings's empirical equation describing forced flow through an orifice in a large wall. That equation determines the volume flux carried by the jet emerging from the aperture; in our case it includes in addition the influence of the impact of the jet on the exterior baffle. Our use of this equation to predict the influence of a small baffled window in a tunnel entrance hood on the compression wave generated by a high-speed train agrees well with measurements made at model scale at speeds ~300 km/h. Similar good agreement with experiment is found for a baffled long slit window for speeds $\sim300-400$ km/h, after first representing the long window by an array of smaller, hydrodynamically coupled windows of the same total area. It is now appropriate to consider the incorporation of this representation of an exterior baffle into more general compression wave prediction schemes, such as that proposed by Howe et al. (2006).

Acknowledgements

The authors express their gratitude to Mr T. Suzuki of Tess Co. Ltd. and Dr T. Fukuda of RTRI for their assistance with the model scale experiments.

Appendix A. Green's function

Put

$$G(\mathbf{x},\mathbf{y};t-\tau)=-\frac{1}{2\pi}\int_{-\infty}^{\infty}\bar{G}(\mathbf{x},\mathbf{y};\omega)\mathrm{e}^{-\mathrm{i}\omega(t-\tau)}\,\mathrm{d}\omega, \tag{A.1}$$

where $\bar{G}$ satisfies the inhomogeneous Helmholtz equation $(\nabla^2+\kappa_0^2)\bar{G}=\delta(\mathbf{x}-\mathbf{y})$, $\kappa_0=\omega/c_0$. The solution of this equation is required at points $\mathbf{x}$ within the duct of Fig. A1 (of cross-sectional area $\mathscr{A}$) at distances $|x_1|\gg\sqrt{\mathscr{A}}$ from the aperture when the source point $\mathbf{y}$ is in the neighbourhood of the aperture, and for the *compact* limit where the characteristic wavelength of the sound is large relative to $\sqrt{\mathscr{A}}$.

Only plane waves can propagate within the duct when $\kappa_0\sqrt{\mathscr{A}}\ll 1$ (Pierce, 1989). $\bar{G}(\mathbf{x},\mathbf{y};\omega)$ is then readily determined from the solution of the reciprocal problem in which the source is at $\mathbf{x}$ within the duct and the solution $\bar{G}(\mathbf{y},\mathbf{x};\omega)$ is sought as a function of $\mathbf{y}$ near the aperture. The solution of the direct problem is then obtained from the reciprocal relation $\bar{G}(\mathbf{x},\mathbf{y};\omega)=\bar{G}(\mathbf{y},\mathbf{x};\omega)$ (Rayleigh, 1945). When $\kappa_0\sqrt{\mathscr{A}}$ is small the potential due to a source at $\mathbf{x}$ in the reciprocal problem is equal to $\mathrm{e}^{\mathrm{i}\kappa_0|y_1-x_1|}/2\mathrm{i}\kappa_0\mathscr{A}$ when $|x_1-y_1|\gg\sqrt{\mathscr{A}}$ in a duct unbounded in both directions. To fix ideas, consider the case where the observer in the direct problem is in $x_1<0$ to the left of the aperture in Fig. A1. On the right of the source ($y_1>x_1$), but at distances $\gg\sqrt{\mathscr{A}}$ from the aperture, we write

$$\bar{G}(\mathbf{y},\mathbf{x};\omega)=\frac{\mathrm{e}^{-\mathrm{i}\kappa_0 x_1}}{2\mathrm{i}\kappa_0\mathscr{A}}\{\mathrm{e}^{\mathrm{i}\kappa_0 y_1}+\mathscr{R}\mathrm{e}^{-\mathrm{i}\kappa_0 y_1}\}, \tag{A.2}$$

where the complex coefficient $\mathscr{R}$ determines the amplitude and phase of the wave reflected from the region of the aperture. Now $\kappa_0 y_1$ is small near the aperture, and therefore just to the left of the aperture we have approximately

$$\bar{G}(\mathbf{y},\mathbf{x};\omega)\approx\frac{\mathrm{e}^{-\mathrm{i}\kappa_0 x_1}}{2\mathrm{i}\kappa_0\mathscr{A}}\{1+\mathscr{R}+\mathrm{i}\kappa_0 y_1(1-\mathscr{R})\},\quad \sqrt{\mathscr{A}}\ll|y_1|\ll 1/\kappa_0. \tag{A.3}$$

Similarly, in the duct on the right of the aperture

$$\bar{G}(\mathbf{y},\mathbf{x};\omega)=\frac{\mathrm{e}^{-\mathrm{i}\kappa_0 x_1}}{2\mathrm{i}\kappa_0\mathscr{A}}\mathscr{T}\mathrm{e}^{\mathrm{i}\kappa_0 y_1}\approx\frac{\mathrm{e}^{-\mathrm{i}\kappa_0 x_1}}{2\mathrm{i}\kappa_0\mathscr{A}}\mathscr{T}\{1+\mathrm{i}\kappa_0 y_1\},\quad \sqrt{\mathscr{A}}\ll|y_1|\ll 1/\kappa_0, \tag{A.4}$$

where $\mathscr{T}$ is a suitable transmission coefficient.

When the acoustic wavelength is much larger than the duct width the motion through the aperture becomes identical to that of an irrotational, reciprocating incompressible flow, where we can write

$$\bar{G}(\mathbf{y},\mathbf{x};\omega)\approx\frac{\mathrm{e}^{-\mathrm{i}\kappa_0 x_1}}{2\mathrm{i}\kappa_0\mathscr{A}}(\mathscr{B}+\mathscr{C}\varphi^*(\mathbf{y})), \tag{A.5}$$

where $\mathscr{B}$, $\mathscr{C}$ are constants and $\varphi^*(\mathbf{y})$ is a velocity potential that represents incompressible irrotational flow out of the duct through the aperture, with asymptotic behaviours given in Eq. (2.7) of the main text. The value of ℓ in (2.7) varies

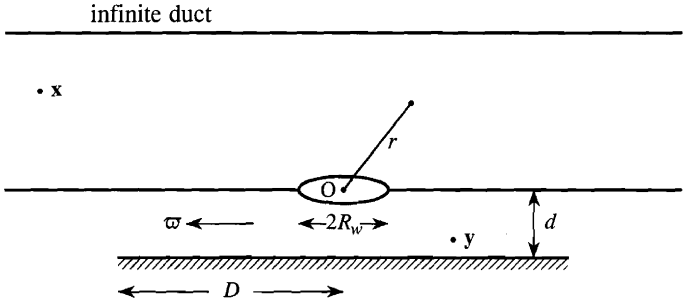

Fig. A1. Infinite duct with circular wall aperture and exterior circular wall element of radius D.

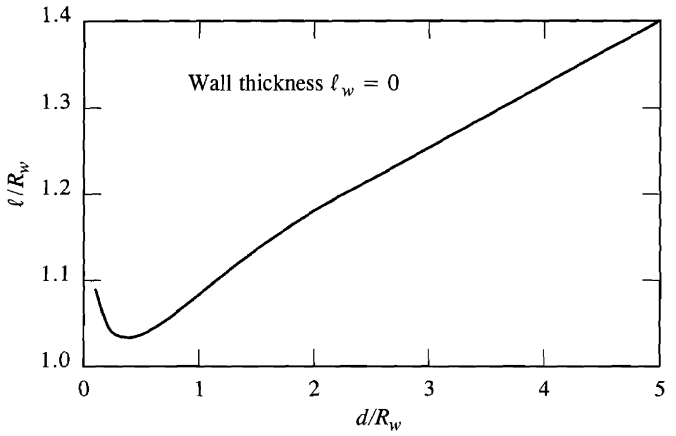

Fig. A2. Variation of the end correction ℓ of the baffled aperture with the external wall standoff distance d when the cylinder wall thickness $\ell_w = 0$.

with the standoff distance d. Its variation as a function of d/R_w is illustrated in Fig. A2 for $\ell_w = 0$, calculated from the formula

$$\ell = \int_{-\infty}^{\varpi} \frac{\partial \varphi^*}{\partial s}\,\mathrm{d}s - \frac{\mathscr{A}_w}{2\pi d}\ln\left(\frac{\varpi}{R_w}\right),$$

where s is distance along an integration contour that starts at $|s| \gg R_w$ within the duct, passes through the aperture and terminates at a radial distance $s \sim \varpi \gg R_w$ in the gap. The figure shows how ℓ increases with d/R_w, formally approaching $\ell \sim (\pi/2)R_w$ as $d/R_w \to \infty$, the same as for a circular aperture in a plane wall of infinitesimal thickness in the absence of other boundaries. It also increases when d is very small, because $\partial\varphi^*/\partial s$ must become very large within the aperture to maintain a constant volume flux. The end correction for $\ell_w > 0$ is approximately given by adding ℓ_w to the value shown in Fig. A2.

It is assumed that the characteristic wavelength is large compared to the radius D of the baffle, and that the radiation of sound from its circumference into the ambient medium is negligible, so that $\bar{G}(\mathbf{y}, \mathbf{x}; \omega) = 0$ there. Then

$$\mathscr{B} = -\mathscr{C}\left[\frac{\mathscr{A}_w}{2\pi d}\ln\left(\frac{D}{R_w}\right) + \ell\right],$$

and Eq. (A.5) becomes

$$\bar{G}(\mathbf{y}, \mathbf{x}; \omega) \approx \frac{\mathrm{e}^{-\mathrm{i}\kappa_0 x_1}}{2\mathrm{i}\kappa_0 \mathscr{A}}\,\mathscr{C}\{\varphi^*(\mathbf{y}) - \mathscr{L}\} \quad \text{where } \mathscr{L} = \frac{\mathscr{A}_w}{2\pi d}\ln\left(\frac{D}{R_w}\right) + \ell. \tag{A.6}$$

The values of the remaining constants $\mathscr{R}$, $\mathscr{T}$ and $\mathscr{C}$ are now found by equating values of the potential and volume flux in the regions of overlap of approximations (A.3), (A.4) and (A.6), making use of the relations (2.7). In this way we find

$$\mathscr{T} = 1 + \mathscr{R} = -\mathscr{C}\mathscr{L} = \frac{\kappa_0}{\left(\kappa_0 + \dfrac{\mathrm{i}\mathscr{A}_w}{2\mathscr{L}\mathscr{A}}\right)}. \tag{A.7}$$

In particular Eqs. (A.1), (A.6) and the reciprocal theorem now show that for source points $\mathbf{y}$ in the vicinity of the aperture

$$G(\mathbf{x}, \mathbf{y}, t-\tau) \approx \frac{\{\varphi^*(\mathbf{y}) - \mathscr{L}\}}{4\pi\mathrm{i}\mathscr{L}\mathscr{A}}\int_{-\infty}^{\infty} \frac{\mathrm{e}^{-\mathrm{i}\omega(t-\tau+x_1/c_0)}\,\mathrm{d}\omega}{\kappa_0 + \mathrm{i}\mathscr{A}_w/2\mathscr{L}\mathscr{A}}, \quad x_1 \ll -\sqrt{\mathscr{A}}. \tag{A.8}$$

The same result with $-x_1$ replaced by $+x_1$ is obtained when the observer is at $x_1 \gg \sqrt{\mathscr{A}}$ to the right of the aperture. In both cases, therefore, we find

$$G(\mathbf{x}, \mathbf{y}, t-\tau) \approx \frac{c_0}{2\mathscr{A}}\left\{1 - \frac{\varphi^*(\mathbf{y})}{\mathscr{L}}\right\}\mathrm{H}\left(t - \tau - \frac{|\mathbf{x}|}{c_0}\right)\exp\left\{\frac{-c_0\mathscr{A}_w}{2\mathscr{L}\mathscr{A}}\left(t - \tau - \frac{|\mathbf{x}|}{c_0}\right)\right\}, \quad |\mathbf{x}| \gg \sqrt{\mathscr{A}}. \tag{A.9}$$

This represents the potential produced at $\mathbf{x}$ at time t in the duct at large distances from the aperture by a point source $\delta(\mathbf{x}-\mathbf{y})\delta(t-\tau)$ in the immediate vicinity of the aperture. When $|\mathbf{y}| \equiv r \gg R_w$ in the duct the geometrical details of the aperture become unimportant, because $\varphi^*(\mathbf{y})/\mathscr{L} \to 0$ and

$$G(\mathbf{x},\mathbf{y},t-\tau) \approx \frac{c_0}{2\mathscr{A}}\,\mathrm{H}\left(t-\tau-\frac{|\mathbf{x}|}{c_0}\right)\exp\left\{\frac{-c_0\mathscr{A}_w}{2\mathscr{L}\mathscr{A}}\left(t-\tau-\frac{|\mathbf{x}|}{c_0}\right)\right\}, \quad |\mathbf{x}| \gg \sqrt{\mathscr{A}}. \tag{A.10}$$

In the absence of the aperture the low frequency potential produced by a point source at $\mathbf{y}\sim 0$ would be

$$G(\mathbf{x},\mathbf{y},t-\tau) \approx \frac{c_0}{2\mathscr{A}}\,\mathrm{H}\left(t-\tau-\frac{|\mathbf{x}|}{c_0}\right), \quad |\mathbf{x}| \gg \sqrt{\mathscr{A}}.$$

The exponential factors in approximations (A.9), (A.10) account for the gradual decay of this step wave to the rear of the two wavefronts propagating to $x_1 = \pm\infty$ because of the presence of the aperture and the vanishing of G at the opening to the free space ambient fluid at $\varpi = D$.

Appendix B. Effective jet contraction ratio

Consider nominally steady, free-streamline flow from the duct through the baffled wall aperture driven by a *constant* and uniform excess pressure p_0 within the duct. According to Bernoulli's equation the asymptotic speed of the wall jet flow along the baffle is $U_\sigma = \sqrt{2p_0/\rho_0}$. The mean flow speed V out of the duct in a plane spanning the aperture is $V = \sigma U_\sigma$, where σ is the discharge coefficient, i.e. the effective area-contraction ratio of the jet outflow.

B.1. Two-dimensional jet

The dependence of σ on the baffle standoff distance d is readily determined in the case of flow from a slit aperture, where the whole motion may be assumed to be two-dimensional and calculated by the complex variable method of free-streamline theory (Lamb, 1932; Birkhoff and Zarantonello, 1957; Gurevich, 1965). Fig. B1(a) illustrates the calculated form of the free streamlines in the simplest case of steady two-dimensional, incompressible flow from the half-space $x_3 > 0$ through a slit aperture occupying the interval $-h < x_1 < h$ in a thin wall at $x_3 = 0$. The flow discharges against an infinite plane wall at $x_3 = -d$, forming symmetric wall jets of asymptotic width σh.

The calculated dependence of σ on $d/2h$ is shown in Fig. B1(b); it reveals that σ may be assumed to have attained its asymptotic value of 0.61 for $d > 2h$. There is no simple formula that relates σ and $d/2h$, but the following argument leads to an excellent interpolation formula (whose predictions are shown dotted in the figure):

(a) When $d/2h \to 0$ the shape and size of each of the symmetrical jets must be the same as that predicted for flow into a two-dimensional *Borda mouthpiece* (Lamb, 1932; Birkhoff and Zarantonello, 1957; Gurevich, 1965; Batchelor, 1967). In this limit the asymptotic jet thickness is $\sigma h = d/2$, so that

$$\sigma \to \frac{d}{2h} \quad \text{as} \quad \frac{d}{2h} \to 0.$$

(b) When $d/2h \gg 1$ the asymptotic jet width of contraction ratio $\sigma \approx 0.61$ is attained before impact with the wall, and therefore

$$\sigma \to \sigma_{\max} \approx 0.61 \quad \text{as} \quad \frac{d}{2h} \to \infty.$$

The results (a) and (b) actually determine not only the limiting values of σ as $d/2h \to 0, \infty$, but also the *slopes* of the functional dependence. Because the upper limiting value is attained essentially for $d/2h > 1$, this suggests the use of the following interpolation formula:

$$\sigma = \sigma_{\max}\,\mathrm{erf}\left(\frac{\sqrt{\pi}}{2\sigma_{\max}}\frac{d}{2h}\right), \quad \sigma_{\max} \approx 0.61. \tag{B.1}$$

This is plotted as the dotted curve in Fig. B1(b), where it is seen to provide an excellent working approximation to the exact dependence of σ on $d/2h$.

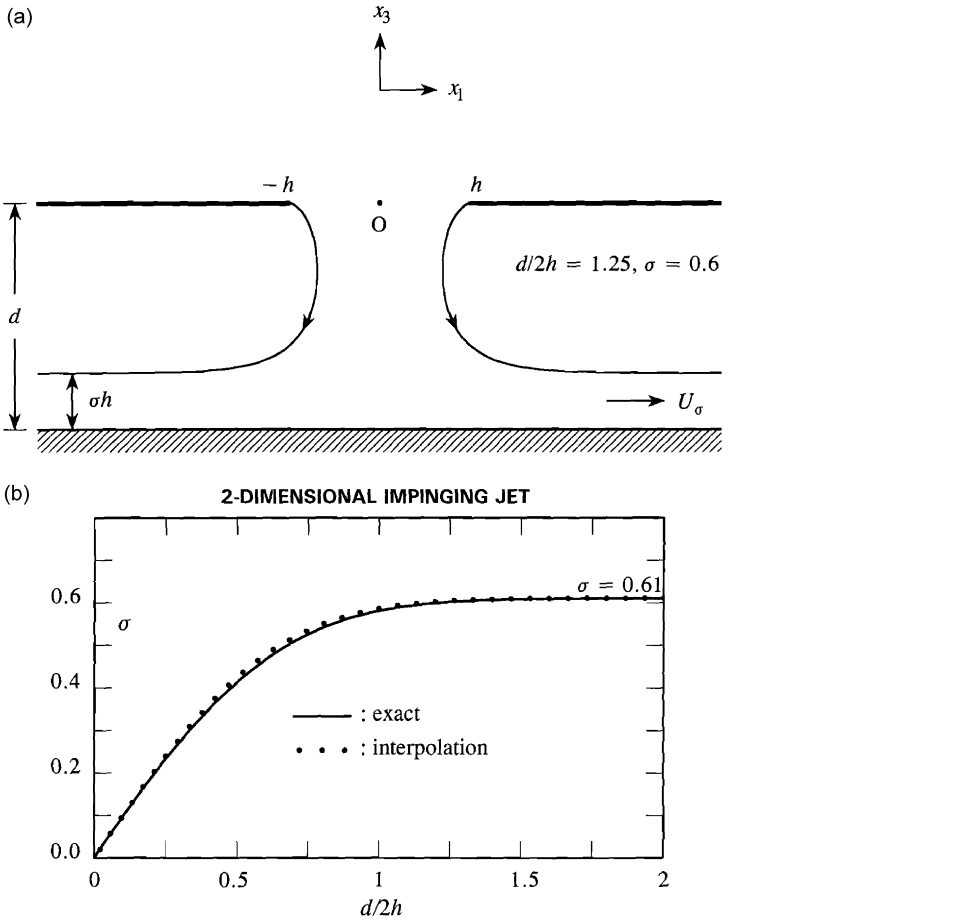

Fig. B1. (a) Two-dimensional free-streamline flow from an aperture of width $2h$ in a thin wall into a gap of width d between the wall and an infinite baffle panel. (b) Calculated dependence of σ on $d/2h$ (——) and the dependence (•••) given by the interpolation formula (B.1).

B.2. Axisymmetric jet

The corresponding free-streamline area-contraction ratio of a circular jet impinging on a baffle plate is not amenable to analytical treatment, although the free jet has been investigated numerically [e.g. Southwell (1946), Southwell and Vaisey (1946), Garabedian (1956), Birkhoff and Zarantonello (1957), and Bergthorson et al. (2005)] have discussed the impinging jet at low Reynolds numbers. It will be sufficient here to develop an approximate interpolation formula that gives σ as a function of the nondimensional standoff distance d/R_w, analogous to Eq. (B.1) for the two-dimensional jet.

To do this we note that

(a) when $d/R_w \to 0$ the *Borda mouthpiece* limit implies that the volume flux $\pi R_w^2 \sigma U_\sigma$ through the aperture must equal $2\pi R_w \times d/2 \times U_\sigma$, so that

$$\sigma \to \frac{d}{R_w} \quad \text{as} \quad \frac{d}{R_w} \to 0;$$

(b) when $d/R_w \gg 1$ the asymptotic jet contraction ratio $\sigma \approx 0.62$ is attained before impact with the wall, and therefore

$$\sigma \to \sigma_{\max} \approx 0.62 \quad \text{as} \quad \frac{d}{R_w} \to \infty.$$

These limiting values of σ determine the following interpolation formula analogous to (B.1):

$$\sigma = \sigma_{\max} \operatorname{erf}\left(\frac{\sqrt{\pi}}{2\sigma_{\max}}\frac{d}{R_w}\right), \quad \sigma_{\max} \approx 0.62. \tag{B.2}$$

The independent variable d is scaled by the radius R_w of the aperture, whereas in two dimensions the corresponding length scale is $2h$. This is in accord with the observation that relaxation to uniform conditions occurs more rapidly in three dimensions than in two.

Cummings (1984, 1986) showed from a comparison with experiment that for the approximate calculation of unsteady flow involving free jets better agreement with experiment is obtained by taking $\sigma = 0.75$ instead of the usual steady jet value $\sim$0.62. We shall introduce the same correction for the unsteady jet impingement problem. To do this approximation (B.2) must be scaled-up for use in Eqs. (2.18) and (4.13) when, respectively, $V(t)$, $V_k(t) > 0$. This is done by replacing the first, multiplicative factor $\sigma_{\max}$ in (B.2) by 0.75, but leaving the value of $\sigma_{\max}$ *unchanged* in the argument of the error function. This yields formula (2.17) of the main text.

References

Baker, B.B., Copson, E.T., 1969. The Mathematical Theory of Huygen's Principle, second ed. Oxford University Press, Oxford.

Batchelor, G.K., 1967. An Introduction to Fluid Dynamics. Cambridge University Press, Cambridge.

Benade, A.H., 1976. Fundamentals of Musical Acoustics. Oxford University Press, Oxford.

Bergthorson, J.M., Sone, K., Mattner, T.W., Dimotakis, P.E., Goodwin, D.G., Meiron, D.I., 2005. Impinging laminar jets at moderate Reynolds numbers and separation distances. Physical Review E 72 (6) Article No. 066307.

Birkhoff, G., Zarantonello, E.H., 1957. Jets, Wakes and Cavities. Academic Press, New York.

Crighton, D.G., 1985. The Kutta condition in unsteady flow. Annual Review of Fluid Mechanics 17, 411–445.

Crighton, D.G., Dowling, A.P., Ffowcs Williams, J.E., Heckl, M., Leppington, F.G., 1992. Modern Methods in Analytical Acoustics (Lecture Notes). Springer, London.

Cummings, A., 1984. Acoustic nonlinearities and power losses at orifices. AIAA Journal 22, 786–792.

Cummings, A., 1986. Transient and multiple frequency sound transmission through perforated plates at high amplitude. Journal of the Acoustical Society of America 79, 942–951.

Garabedian, P.R., 1956. Calculation of axially symmetric cavities and jets. Pacific Journal of Mathematics 6, 611–684.

Gurevich, M.I., 1965. Theory of Jets in Ideal Fluids. Academic Press, New York.

Howe, M.S., 1979a. Attenuation of sound in a low Mach number nozzle flow. Journal of Fluid Mechanics 91, 209–230.

Howe, M.S., 1979b. On the theory of unsteady high Reynolds number flow through a circular aperture. Proceedings of the Royal Society of London A 366, 205–233.

Howe, M.S., 1998a. Acoustics of Fluid–Structure Interactions. Cambridge University Press, Cambridge.

Howe, M.S., 1998b. The compression wave produced by a high-speed train entering a tunnel. Proceedings of the Royal Society of London A 454, 1523–1534.

Howe, M.S., 1999. Review of the theory of the compression wave generated when a high-speed train enters a tunnel. Proceedings of the Institution of Mechanical Engineers Part F, Journal of Rail and Rapid Transit 213 (F2), 89–104.

Howe, M.S., 2003. Theory of Vortex Sound. Cambridge University Press, Cambridge.

Howe, M.S., 2005. On the role of separation in compression wave generation by a train entering a tunnel hood with a window. Institute of Mathematics and its Applications, Journal of Applied Mathematics 70, 400–418.

Howe, M.S., 2007. The genetically optimized tunnel-entrance hood. Journal of Fluids and Structures 23, 1231–1250.

Howe, M.S., Iida, M., 2003. Influence of separation on the compression wave generated by a train entering a tunnel. International Journal of Aeroacoustics 2, 13–33.

Howe, M.S., McGowan, R.S., 2007. Sound generated by aerodynamic sources near a deformable body, with application to voiced speech. Journal of Fluid Mechanics 592, 367–392.

Howe, M.S., Iida, M., Fukuda, T., Maeda, T., 2000. Theoretical and experimental investigation of the compression wave generated by a train entering a tunnel with a flared portal. Journal of Fluid Mechanics 425, 111–132.

Howe, M.S., Iida, M., Fukuda, T., Maeda, T., 2003a. Aeroacoustics of a tunnel-entrance hood with a rectangular window. Journal of Fluid Mechanics 487, 211–243.

Howe, M.S., Iida, M., Fukuda, T., 2003b. Influence of an unvented tunnel entrance hood on the compression wave generated by a high-speed train. Journal of Fluids and Structures 17, 833–853.

Howe, M.S., Iida, M., Maeda, T., Sakuma, Y., 2006. Rapid calculation of the compression wave generated by a train entering a tunnel with a vented hood. Journal of Sound and Vibration 297, 267–292.

Hughes, I.J., Dowling, A.P., 1990. The absorption of sound by perforated linings. Journal of Fluid Mechanics 218, 299–336.

Lamb, H., 1932. Hydrodynamics, sixth ed. Cambridge University Press, Cambridge.

Landau, L.D., Lifshitz, E.M., 1987. Fluid Mechanics, second ed. Pergamon, Oxford.

Leppington, F.G., 1982. On the theory of woodwind finger holes. Journal of Sound and Vibration 83, 521–532.

Lighthill, M.J., 1952. On sound generated aerodynamically Part I: general theory. Proceedings of the Royal Society of London A 211, 564–587.

Maeda, T., 2002. Micropressure waves radiating from a Shinkansen tunnel portal. In: Krylov, V.V. (Ed.), Noise and Vibration from High Speed Trains. Thomas Telford (Chapter 7).

Maeda, T., Matsumura, T., Iida, M., Nakatani, K., Uchida, K., 1993. Effect of shape of train nose on compression wave generated by train entering tunnel. In: Iguchi, M. (Ed.), Proceedings of the International Conference on Speedup Technology for Railway and Maglev Vehicles, Yokohama, Japan, 22–26 November, pp. 315–319.

Ozawa, S., Maeda, T., 1988. Model experiment on reduction of micro-pressure wave radiated from tunnel exit. In: Emori, R.I. (Ed.), Proceedings of the International Symposium on Scale Modeling, Tokyo, Seikei University, 18–22 July. Japan Society of Mechanical Engineers, pp. 33–37.

Ozawa, S., Maeda, T., 1998. Tunnel entrance hoods for reduction of micro-pressure wave. Quarterly Report of the Railway Technical Research Institute 29 (3), 134–139.

Ozawa, S., Uchida, T., Maeda, T., 1978. Reduction of micro-pressure wave radiated from tunnel exit by hood at tunnel entrance. Quarterly Report of the Railway Technical Research Institute 19 (2), 77–83.

Ozawa, S., Maeda, T., Matsumura, T., Uchida, K., Kajiyama, H., Tanemoto, K., 1991. Countermeasures to reduce micro-pressure waves radiating from exits of Shinkansen tunnels. In: Haerter, A. (Ed.), Aerodynamics and Ventilation of Vehicle Tunnels. Elsevier Science Publishers, Amsterdam, pp. 253–266.

Pierce, A.D., 1989. Acoustics, An Introduction to its Principles and Applications. American Institute of Physics, New York.

Rayleigh, L., 1926. The Theory of Sound, vol. 2. Macmillan, London.

Salikuddin, M., 1990. Acoustic behaviour of orifice plates and perforated plates with reference to low-frequency sound absorption. Journal of Sound and Vibration 139, 361–382.

Salikuddin, M., Plumlee, H.E., 1980. Low frequency sound absorption of orifice plates, perforated plates and nozzles. AIAA Paper 80-0991.

Southwell, R.V., 1946. Relaxation Methods in Theoretical Physics. Oxford University Press, Oxford.

Southwell, R.V., Vaisey, G., 1946. Relaxation methods applied to engineering problems. XII: fluid motions characterized by 'free' stream-lines. Philosophical Transactions of the Royal Society of London A 240, 117–161.

Vér, I.L., 1990. Practical examples of noise and vibration control: case history of consulting projects. Noise Control Engineering Journal 35, 115–125.